2025 1st Season Stock Assessment of Falkland calamari (*Doryteuthis gahi*)

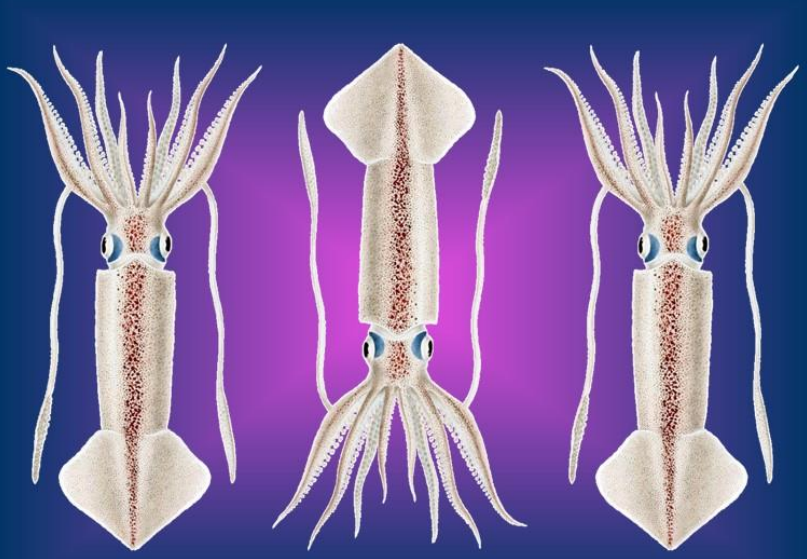

S1 – 2025 – LOL

Skeljo F · Winter A

Fisheries Department
Directorate of Natural Resources
Falkland Islands Government
Stanley, Falkland Islands

July 2025

Participating Scientific Staff

Frane Skeljo (PhD, Senior Stock Assessment Scientist)
Andreas Winter (PhD, Head of Science)

Acknowledgements

We thank all the observers and researchers that have contributed to the data used in this stock assessment report.

© Crown Copyright 2025

For citation purposes this publication should be referenced as follows:

Skeljo F, Winter A. 2025. Stock assessment – Falkland calamari *Doryteuthis gahi* 1st season 2025. Technical Document, Falkland Islands Fisheries Department. 34 p.

Distribution: Public Domain

Reviewed and approved by:

James Wilson Date: July 2025
Director of Natural Resources

Index

Summary

1) The 1st season 2025 *Doryteuthis gahi* fishery (C licence) started on March 1st and finished on April 27th following a closure order. Two grid squares in the north (XPAP and XQAP) were closed on April 10th, and three grid squares in the south (XVAK, XVAL, XUAL) on April 25th; the closures were in response to observed small squid sizes and remained in place until the season end.
2) 37,592 tonnes of *D. gahi* were reported caught in the 2025 C-license fishery, giving an average CPUE of 41.7 tonnes per vessel-day. Both total catch and average CPUE were lowest among the most recent five first seasons, although still above long-term average. 33.4% of *D. gahi* catch and 28.8% of fishing effort were taken north of 52°S; 66.6% of *D. gahi* catch and 71.2% of fishing effort were taken south of 52°S.
3) In the north sub-area, one immigration peak was inferred on March 1st (the start of the season). In the south sub-area, four immigration peaks were inferred on March 1st (the start of the season), March 16th, March 27th, and April 5th.
4) 26,717 tonnes of *D. gahi* (95% CI: 20,192 – 38,517 tonnes) were estimated to have immigrated into the Loligo Box after the start of the first season 2025. Net emigration of 2,892 tonnes was estimated in the north sub-area and net immigration of 29,609 tonnes in the south sub-area.
5) 16,272 tonnes of *D. gahi* (95% CI: 12,395 – 24,009 tonnes) were estimated to remain in the Loligo Box at the end of first season 2025 (hereafter: escapement biomass). The risk of *D. gahi* escapement biomass at the end of the season being less than 10,000 tonnes was calculated as <0.1%.

1. Introduction

The first season (C licence) of the 2025 *Doryteuthis gahi* fishery (Patagonian longfin squid – colloquially *Loligo*) started on March 1st and finished on April 27th following a closure order. Two grid squares in the north (XPAP and XQAP) were closed on April 10th, and three grid squares in the south (XVAK, XVAL, XUAL) on April 25th; the closures were in response to observed small squid sizes and remained in place until the season end. At the season start, eight C-licensed vessels were required to embark a Marine Mammal Observer (hereafter: MRAG observer) to monitor presence and incidental capture of pinnipeds. Approximately halfway through the season, these observers embarked the remaining eight vessels of the fleet for the remainder of the season. Seal exclusion devices (SEDs) were mandatory on all vessels for the duration of the season. Ultimately, 0 pinniped mortalities and 1 live release of a South American fur seal *Arctocephalus australis* were reported for the season.

The total reported *D. gahi* catch under first season C licence was 12,514 north + 24,978 south = 37,492 tonnes, corresponding to an average CPUE of 41.7 tonnes per vessel-day. Both total catch and average CPUE were the lowest among the most recent five first seasons (2021 to 2025), although still above the long-term average (Table 1).

Assessment of the Falkland Islands *D. gahi* stock was conducted with depletion time-series models as in previous seasons (Agnew et al. 1998, Roa-Ureta and Arkhipkin 2007, Arkhipkin et al. 2008) and in other squid fisheries (cited in Arkhipkin et al. 2021). Because *D. gahi* has an annual life cycle (Patterson 1988, Arkhipkin 1993), stock cannot be derived from

a standing biomass carried over from prior years (Rosenberg et al. 1990, Pierce and Guerra 1994). The depletion model instead calculates an estimate of population abundance over time by evaluating what levels of abundance and catchability must be present to sustain the observed catch rate. Depletion modelling of the *D. gahi* target fishery is used in-season, with the objective of maintaining an escapement biomass of 10,000 tonnes of *D. gahi* at the end of each season as a conservation threshold (Agnew et al. 2002, Barton 2002).

Table 1. *D. gahi* season comparisons since 2004, when catch management was assumed by the FIFD. Season days: total number of calendar days open to licensed *D. gahi* fishing including (since 1st season 2013) optional flex days. Vessel days: aggregate number of licensed *D. gahi* fishing days reported by all vessels for the season. Underlined entries are seasons closed by emergency order.

	1st Season			2nd Season		
	Catch (tonnes)	Season days	Vessel days	Catch (tonnes)	Season days	Vessel days
2004	6,668	45	696	18,064	78	1,202
2005	24,773	45	664	29,662	78	1,167
2006	19,056	50	770	23,231	53	817
2007	17,275	50	779	24,239	63	966
2008	24,877	51	780	26,953	78	1,189
2009	12,794	50	773	17,873	59	923
2010	28,681	50	765	36,998	78	1,169
2011	15,288	50	768	18,726	70	1,099
2012	34,727	51	770	35,026	79	1,095
2013	19,906	53	782	19,620	78	1,196
2014	28,117	59	872	19,656	71	1,100
2015	19,424	66	949	10,190	42	665
2016	22,619	68	1,020	23,090	68	1,004
2017	39,425	68	997	24,085	69	1,000
2018	43,086	69	975	35,828	68	977
2019	55,586	68	953	24,748	43	635
2020	29,116	68	1,012	29,759	69	993
2021	59,499	62	891	34,665	68	979
2022	56,080	68	963	43,216	68	982
2023	52,704	67	972	15,513	31	452
2024	47,588	68	974	0	0	0
2025	37,492	58	899			

2. Methods

2.1. Model updates

Compared to the previous assessment that utilised both the squid commercial size categories reported by the fleet and the size structure reported by observers (Skeljo and Winter 2024), the current assessment utilised only size structure data measured in-season by observers to obtain daily average squid size. The commercial size categories were monitored, but not included in the average-size calculation, as they are relatively less accurate. The commercial size categories used across the fleet are not uniform, and while most are defined by size range, some vessels have the smallest size category defined only by the upper limit (e.g. <9 cm mantle length). In this case, the average size of the squid in the smallest category is ambiguous and could potentially bias the average size estimates. Given the high observer coverage (all 16 vessels across the season, and 9-10 vessels concurrently per day), the observer data were deemed representative of the population size structure.

2.2. Model structure

The depletion model formulated for the Falklands *D. gahi* stock is based on the equivalence:

$$\mathrm{C_{day}} = \mathrm{q} \times \mathrm{E_{day}} \times \mathrm{N_{day}} \times \mathrm{e}^{-\mathrm{M}/2} \quad \textbf{(1)}$$

where *q* is the catchability coefficient, *M* is the instantaneous natural mortality rate, and C_{day}, E_{day}, N_{day} are respectively catch (numbers of squid), fishing effort (numbers of vessels), and abundance (numbers of squid) per day.

In its basic form (DeLury 1947) the depletion model assumes a closed population in a fixed area for the duration of the assessment. However, the assumption of a closed population is imperfectly met in the Falkland Islands fishery, where stock analyses have often shown that *D. gahi* groups arrive in successive waves after the start of the season (Arkhipkin et al. 2021). Arrivals of successive groups are inferred from discontinuities in the CPUE data. Fishing on a single, closed cohort would be expected to yield gradually decreasing CPUE, but gradually increasing average individual sizes, as the squid grow. When instead these data change suddenly, or in contrast to expectation, the immigration of a new group to the population is indicated (Winter and Arkhipkin 2015).

In the event of a new group arrival, the depletion calculation must be modified to account for this influx. Modification is done using a simultaneous algorithm that adds new arrivals on top of the stock previously present, and posits a common catchability coefficient for the entire depletion time-series. If two immigrations are included in the same model (i.e. the stock present from the start plus a new group arrival), then:

$$\mathrm{C_{day}} = \mathrm{q} \times \mathrm{E_{day}} \times \left(\mathrm{N1_{day}} + \left(\mathrm{N2_{day}} \times \mathrm{i2}|_0^1\right)\right) \times \mathrm{e}^{-\mathrm{M}/2} \quad \textbf{(2)}$$

where *i2* is a dummy variable taking the values 0 or 1 if 'day' is before or after the start day of the second immigration. For more than two immigrations, $N3_{day}$, *i3*, $N4_{day}$, *i4*, etc., would be included following the same pattern.

The season depletion likelihood function was calculated as the difference between actual catch numbers reported and catch numbers predicted from the model (Equation **2**), assuming lognormal error distribution and treating the variance as a nuisance parameter eliminated by adopting a modified log-likelihood function as an approximation to the exact lognormal log-likelihood function (Roa-Ureta 2012):

$$\text{-LL} = \left((n\text{Days - 2})/2\right)\times\log\left(\sum_{\text{days}}\left(\log\left(\text{predicted C}_{\text{day}}\right) - \log\left(\text{actual C}_{\text{day}}\right)\right)^2\right) \quad \textbf{(3)}$$

The stock assessment was set in a Bayesian framework, whereby results of the season depletion model are conditioned by prior information on the stock; in this case, the information from the pre-season survey. The catchability coefficient prior was considered to be lognormally distributed, and the log-likelihood function was expressed as:

$$\text{-LL} = \log(\sigma_{\text{prior q}}) + 0.5 \times \left(\frac{\log(\text{depletion q}) - \mu_{\text{prior q}}}{\sigma_{\text{prior q}}}\right)^2 \quad \textbf{(4)}$$

where $_{prior}\ q$ is catchability derived from the pre-season survey, $_{depletion}\ q$ is catchability estimated by the depletion model, and μ and σ are the mean and standard deviation of the prior in log-space. For prior information on catchability to be relevant, both the survey and the season have to be fishing the same stock with the same gear. Catchability, rather than abundance *N*, is used for calculating prior likelihood because catchability informs the entire season time series; whereas *N* from the survey only informs the abundance at the start of the season (referred to as the first immigration) while subsequent immigrations are independent of the abundance that was present during the survey.

The model was optimised by jointly minimising Equations **3** and **4**, using the Nelder-Mead algorithm of the 'optim' function in the package 'stats' implemented in R version 4.1.3 (R Core Team, 2022). Relative weights in the joint optimisation were assigned to Equations **3** and **4** as the converse of their coefficients of variation (CV), i.e., the CV of the prior became the weight of the depletion model and the CV of the depletion model became the weight of the prior. Calculations of the depletion CVs are described in Chapter 5.2. Because a complex model with multiple depletions may converge on a local minimum rather than global minimum, the optimisation was stabilised by running a feed-back loop that set the *q* and *N* parameter outputs of the joint optimisation back into the in-season-only minimisation (Equation **3**), re-calculated the in-season-only minimisation, then re-calculated the joint optimisation, and continued this process until both the in-season minimisation and the joint optimisation remained unchanged.

With actual C_{day}, E_{day} and *M* being fixed parameters, the optimisation of Equation **2** using Equations **3** and **4** produces estimates of *q* and *N1*, *N2*, …, etc. Numbers of squid on the final day (or any other day) of a time series are then calculated as the numbers *N* of the depletion start days discounted for natural mortality during the intervening period, and subtracting cumulative catch also discounted for natural mortality (CNMD). Taking, for example, a two-depletion period:

$$\begin{aligned} \text{N}_{\text{final day}} = {} & \text{N1}_{\text{start dat 1}} \times \text{e}^{-\text{M(final day}-\text{start day 1)}} + \\ & \text{N2}_{\text{start dat 2}} \times \text{e}^{-\text{M(final day}-\text{start day 2)}} - \\ & \text{CNMD}_{\text{final day}} \end{aligned} \quad \textbf{(5)}$$

$$\mathrm{CNMD}_{\mathrm{day\ 1}} = 0$$

$$\mathrm{CNMD}_{\mathrm{day\ x}} = \mathrm{CNMD}_{\mathrm{day\ x-1}} \times \mathrm{e}^{-\mathrm{M}} + \mathrm{C}_{\mathrm{day\ x-1}} \times \mathrm{e}^{-\mathrm{M}/2} \quad \textbf{(6)}$$

Finally, abundance *N* on any given day is multiplied by the fitted average individual squid weight on that day to obtain biomass estimates.

The marginal posterior distributions of the parameters in Bayesian analysis were computed using a Markov Chain Monte Carlo (MCMC) (Gamerman and Lopes 2006), a method that is commonly employed for fisheries assessments (Magnusson et al. 2013). For each tested model, three chains were run; one chain initiated with the parameter values obtained from the joint optimisation of Equations **3** and **4**, one chain initiated with these parameters ×2, and one chain initiated with these parameters ×¼. Each chain was run for 510,000 iterations; the first 10,000 iterations were discarded as burn-in sections (initial phases over which the algorithm stabilises) and the following 500,000 iterations were thinned by a factor of 100 to reduce autocorrelation; the resulting 5,000 values approximate the Bayesian posterior distribution. Individual chains were investigated for evidence of non-convergence using trace plots, chain autocorrelation plots, the single-chain stationarity test of Geweke (1992) and the stationarity and half-width tests of Heidelberger and Welch (1983). Convergence of the three chains for each parameter was tested using Gelman and Rubin's diagnostic $\hat{R}$, based on a comparison of within-chain and between-chain variances (Brooks and Gelman 1998). When convergence was satisfied the three chains were combined as one final set. Equations **5**, **6**, and the multiplication by average individual weight were applied to the CNMD and to each iteration of N values in the final set, and the biomass outcomes from these calculations represent the distribution of the estimate.

Depletion models were calculated separately for north and south sub-areas of the Loligo Box fishing zone, as *D. gahi* sub-stocks emigrate from different spawning grounds and remain to an extent segregated (Arkhipkin and Middleton 2002), although they represent a single intermixed population (Shaw et al. 2004). However, *q* prior was calculated for the north and south sub-areas combined, rather than separately (for details on prior calculation see Chapter 5.1). As fishing tends to start predominantly in one or the other sub-area, rather than the fleet spreading itself evenly, separately computed north and south *q* priors are susceptible to arbitrary differences. Total escapement biomass was defined as the aggregate biomass of *D. gahi* on the last day of the season for north and south sub-areas combined, with north and south posterior distributions added together randomly.

Natural mortality

Natural mortality was parameterised in the depletion model as a time-invariant instantaneous rate, calculated from the Hamel and Cope (2022) longevity-based estimator $M = 5.40 / A_{max}$, with a corresponding log-space prediction error = 0.31 (or CV = 32%; Maunder et al. 2023). Assuming a maximum age of 352 days for *D. gahi* resulted in the mortality rate estimate $M = 0.0153\ \mathrm{day}^{-1}$.

Immigration peaks

The start days of immigrations (arrivals of new *D. gahi* groups) are hereafter referred to as immigration peaks. By definition, squid present on the first day of the season is considered the first immigration peak, even though this is de facto not an in-season immigration. Each

immigration peak marks the start of a new depletion period, as the squid that immigrated are being removed by fishing and natural mortality.

Immigration peaks were judged primarily by daily changes in CPUE, with additional information from sex proportions, maturity, and average individual squid sizes. CPUE was calculated as metric tonnes of *D. gahi* caught per vessel-day. Days were used rather than trawl hours as the basic unit of effort. Commercial vessels do not trawl standardised duration hours, but rather durations that best suit their daily processing requirements. An effort index of days is therefore more consistent (FIFD 2004, Winter and Arkhipkin 2015). Inclusion of additional immigration peaks was also partially evaluated by improvement of the Akaike information criterion (AIC; Akaike 1973), when changes in CPUE, sex proportions, maturity and sizes were ambiguous.

Average individual weights

Daily average individual weight is obtained from length-weight conversion of mantle lengths measured in-season by FIFD and MRAG observers. To smooth day-to-day fluctuations, GAM trends were fitted to daily average individual weights per haul weighted by sample size, and used whenever converting abundance to biomass. North and south sub-areas were calculated separately. For continuity, GAMs were calculated using all pre-season survey and in-season data contiguously.

2.3. Data

Data collection

Fishery self-reporting data was extracted from the electronic logbooks and included catch per haul with the corresponding time, position and depth at the start/end of each haul. Three FIG fishery observers were deployed on four vessels in the fishing season for 65 sampling days[a] (Amukwaya 2025, Ongoro 2025, Orlandi 2025a,b). Throughout the 58 days of the season, 12 days had no FIG fishery observer sampling, 27 days had one FIG fishery observer sampling, and 19 days had two FIG fishery observers sampling. Except for seabird days, FIFD fishery observers were tasked with sampling 200 *D. gahi* at two stations daily and reporting their maturity stages, sex, and lengths to 0.5 cm. Additionally, each FIFD fishery observer reported individual weights of 200 *D. gahi* twice a week. MRAG observers were tasked with measuring 100 unsexed lengths of *D. gahi* per day.

Commercial catch and effort data

899 vessel-days were fished during the season, with a median of 16 vessels per day (mean 15.5). The north sub-area was fished on 39 of 58 season-days, for 33.4% of total catch (12,514.5 tonnes *D. gahi*) and 28.8% of effort (259.1 vessel-days). The south sub-area was fished on 49 of the 58 season-days, for 66.6% of total catch (24,977.6 tonnes *D. gahi*) and 71.2% of effort (639.9 vessel-days) (Figures 1 and 2).

[a] Not counting seabird days (every fourth day).

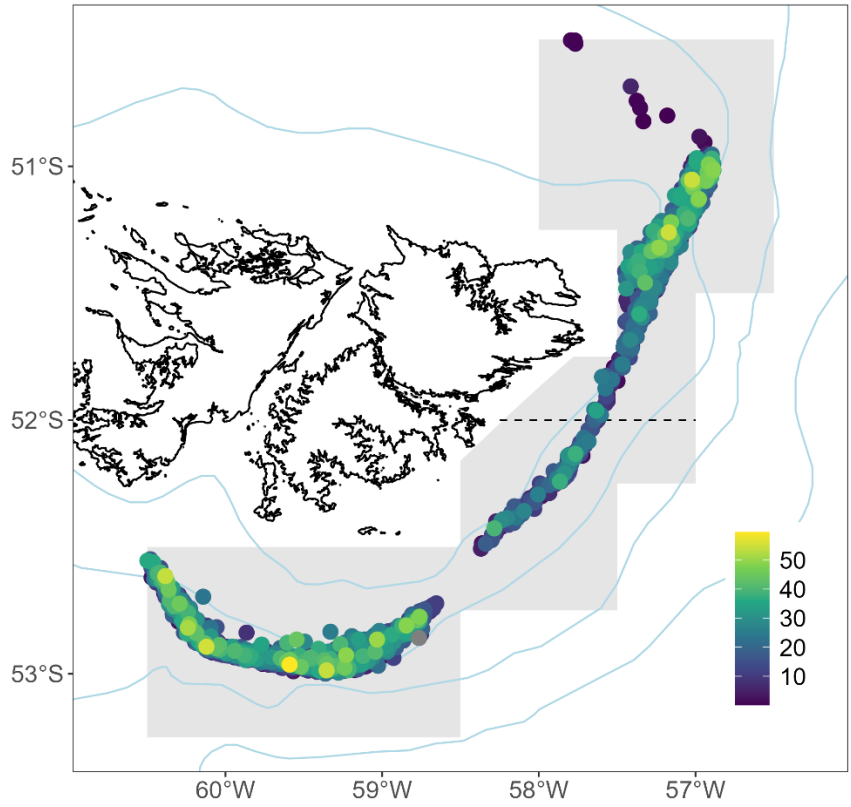

Figure 1. Spatial distribution of trawls (mean coordinate positions) during 1st season 2025, colour-scaled to *D. gahi* catch weight (max. = 59.6 tonnes). 2,000 trawl catches were taken during the season. Grey shading denotes the Loligo Box fishing zone. Dashed line denotes the boundary between north and south assessment sub-areas (52°S parallel).

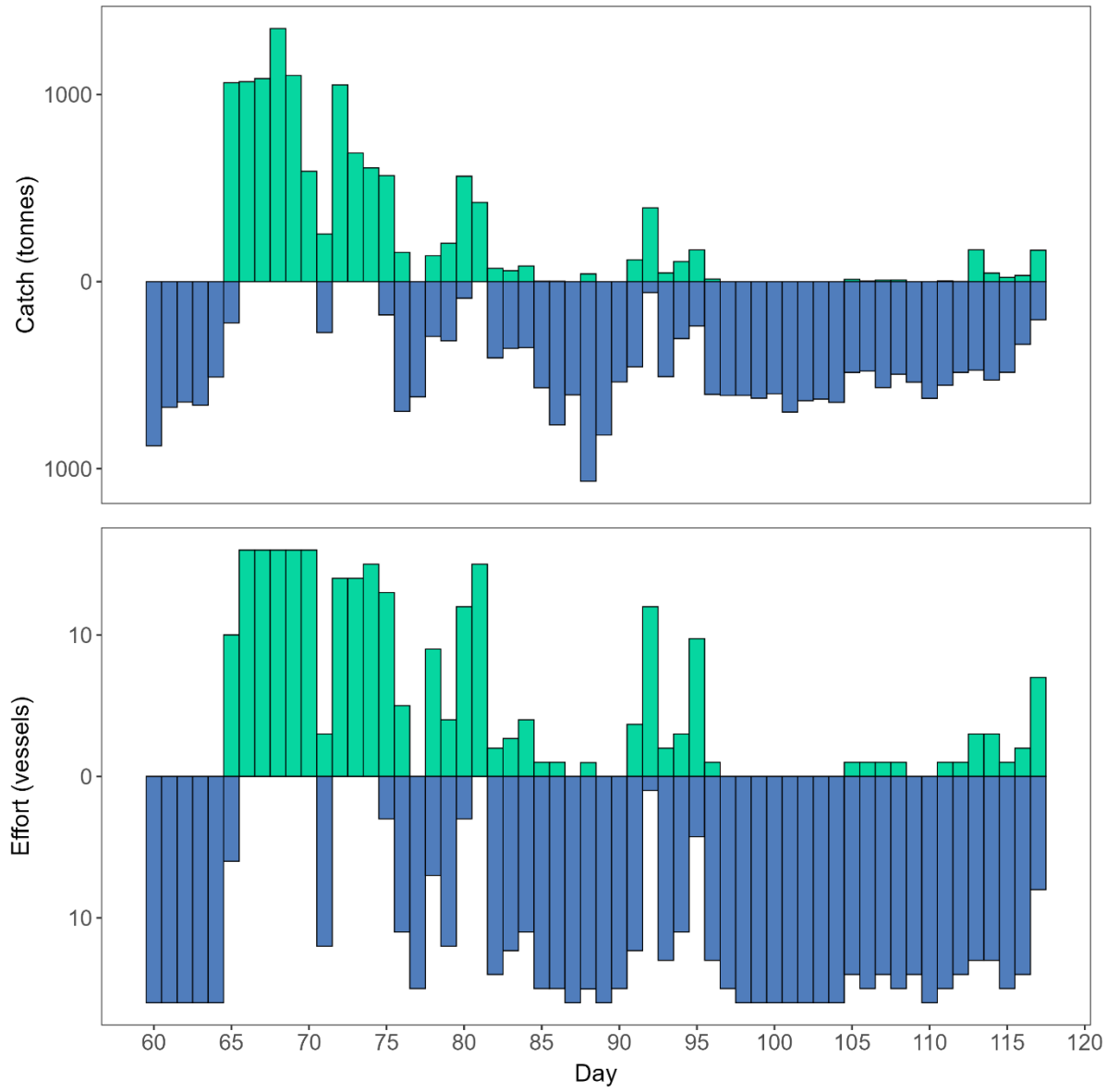

Figure 2. Daily *D. gahi* catch and effort distribution by assessment sub-area north (green) and south (blue) during 1st season 2025. The season was open from March 1st (chronological day 60) with emergency closure on April 27th (chronological day 117).

Length-weight data

The length-weight relationship was calculated as $W = a\,ML^b$ based on the combined mantle length (cm) and body weight (g) data from the first pre-season and season 2024 and 2025, as 2025 data became available progressively with ongoing observer coverage. The final parameterisation of the length-weight relationship included 4,419 measures from 2024 and 5,026 measures from 2025, with estimated parameters a = 0.160 and b = 2.240.

3. Results

3.1. Immigration peaks

One day in the north sub-area and four days in the southsub-area were identified as representing the onset of significant immigrations throughout the season:

- The one immigration peak in the north was set by definition on day 60 (March 1st), the first day of the season with no vessels fishing in the north (Figure 3).
- The first immigration peak in the south was set by definition on day 60 (March 1st), the first day of the season with all sixteen vessels fishing in the south (Figure 3).
- The second immigration peak in the south was identified on day 75 (March 16th) based on a large increase in CPUE (Figure 3) and moderate increase in squid size/maturity (Figure 5).
- The third immigration peak in the south was identified on day 86 (March 27th), based on a moderate increase in CPUE (Figure 3) and large increase in squid size/maturity (Figure 5).
- The fourth immigration peak in the south was identified on day 95 (April 5th), based on a moderate increase in CPUE (Figure 3) and moderate increase in squid size (Figure 5).

In the north sub-area, commercial fishing started on March 6th (day 65) with 10 vessels. CPUE showed some fluctuations but with a clear decreasing trend overall. Some fluctuations were possibly exaggerated due to vessels fishing for fewer hours per day than usual (days 70, 78, 85, 86, 105-108, 111) or very few vessels fishing in the area (days 71, 79, 88, 105-108, 111) (Figure 3). The start of the season is considered the first immigration event by design; no further immigrations were conclusively supported by the data. Therefore, the simplest model with a single immigration peak at the start of the season was preferred.

In the south sub-area, commercial fishing started on March 1st (day 60) with 16 vessels. The start of the season is considered the first immigration event by design. CPUE decreased over the next five days, but then the time series was interrupted as the fleet moved to the north. An isolated fishing day in the south on day 71 suggested no increase in biomass. However, fishing in the south resumed on days 75-76; a large increase in CPUE indicated that second immigration occurred between days 72 and 75 (assigned to day 75). The aggregation was found on the western edge of the Loligo Box and consisted of noticeably larger squid than found earlier in the area. The third immigration occurred approximately two weeks later (between days 85 and 88; assigned to day 86), also on the western edge of the Loligo Box, and was characterised by a large increase in CPUE and large squid. The fourth immigration occurred on day 95 in the west of the Loligo Box and was characterised by a sharp increase in CPUE and the highest average squid size recorded by MRAG observers this season.

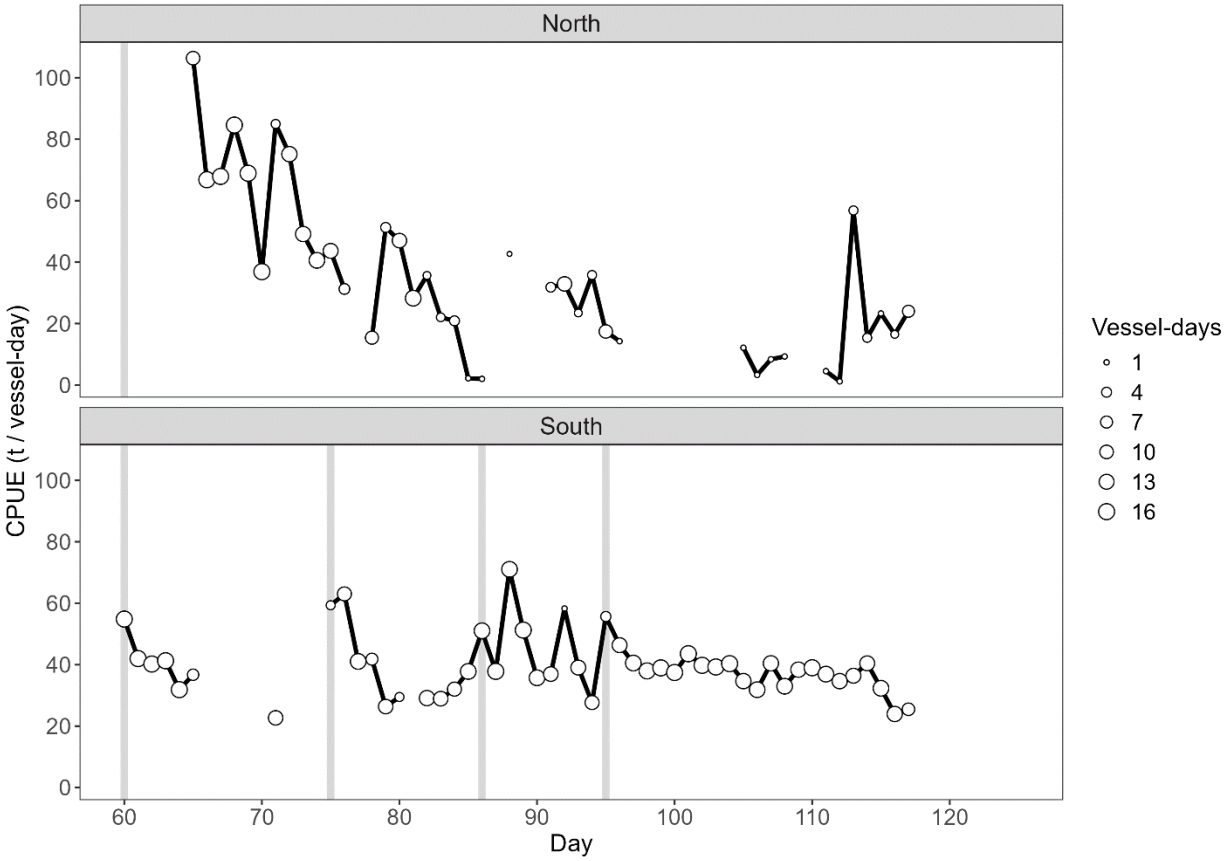

Figure 3. *D. gahi* CPUE time-series in the north and south sub-area during first season 2025. Dot sizes are proportioned to numbers of vessels fishing. Data from consecutive days are joined by line segments. Grey bars: immigration peaks north (day 60) and south (days 60, 75, 86 and 95).

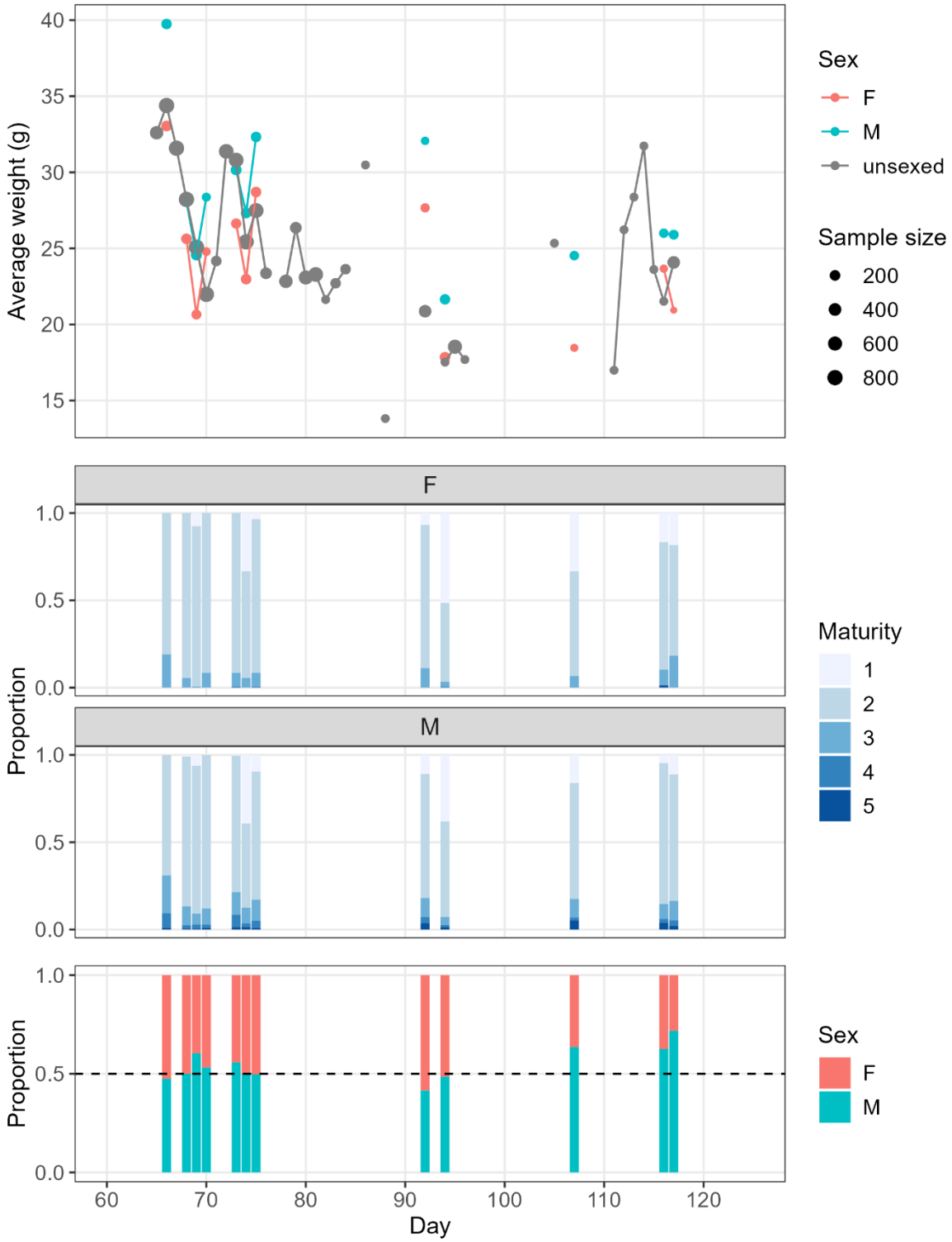

Figure 4. *D. gahi* biological data time-series in the north sub-area. Average individual weights by sex, proportion of maturity stages per sex, and proportion of sexes are from the FIFD observer data. The average weights of unsexed individuals are from the MRAG observer data.

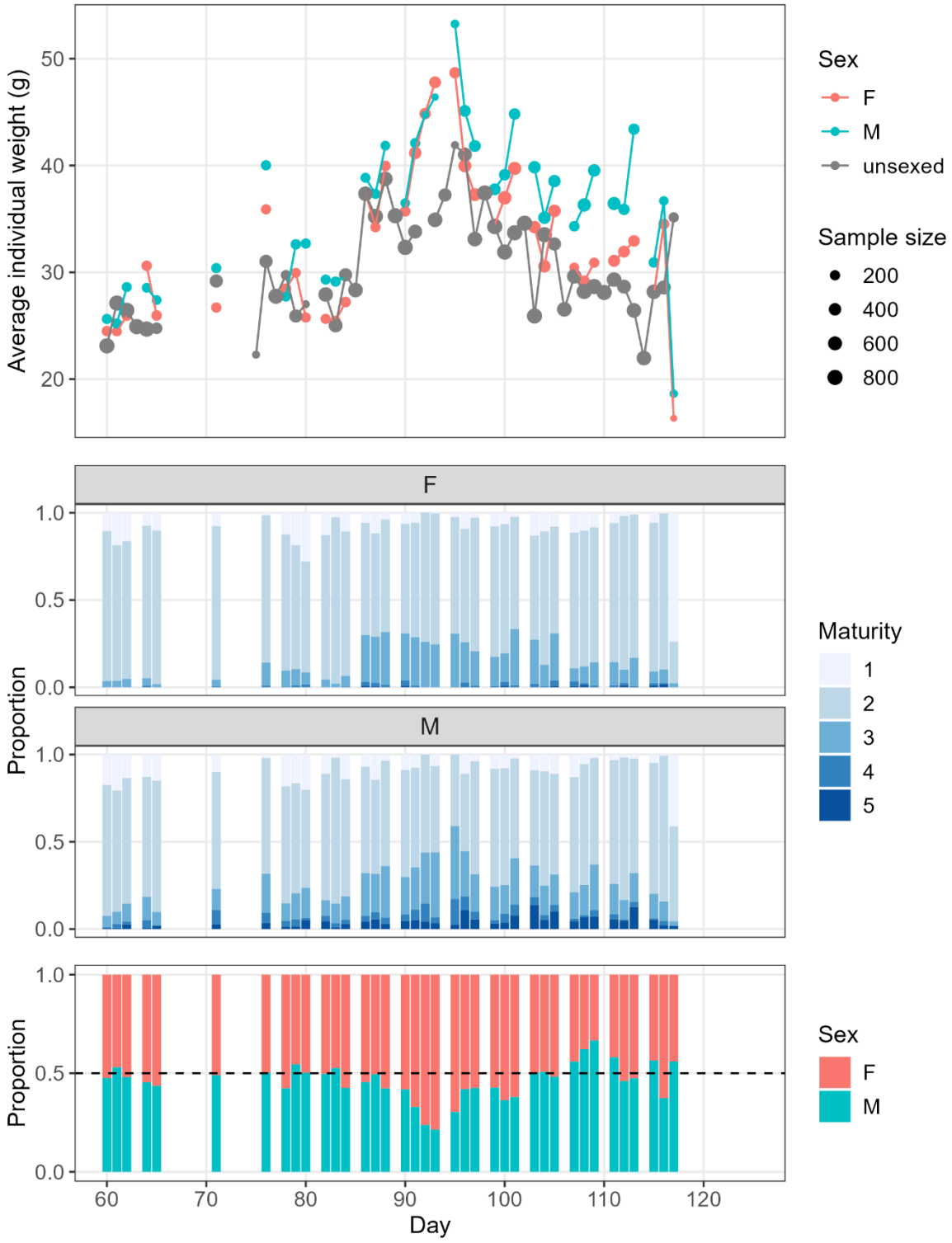

Figure 5. *D. gahi* biological data time-series in the south sub-area throughout the season. Average individual weights by sex, proportion of maturity stages per sex, and proportion of sexes are from the FIFD observer data. The average weights of unsexed individuals are from the MRAG observer data.

3.2. Average individual weights

GAMs fitted to daily average individual weights showed contrasting trends in the north and south sub-areas. In the north, the largest sizes were found at the beginning of the season (fishing in the north started on day 65), followed by a decline in size over the next four weeks (Figure 6). The north was fished infrequently over the last 3 weeks of the season; there appeared to be an increase in squid size towards the season end, but this was likely an artefact of the closure of two grid squares where small-sized squid were found.

In the south, the average size was lowest at the beginning of the season (fishing in the south started on day 60), followed by an increase over the next five weeks (Figure 6). The increase was driven primarily by the immigration of large squid into the southwest of the Loligo Box. Towards the end of the season, the sizes decreased again.

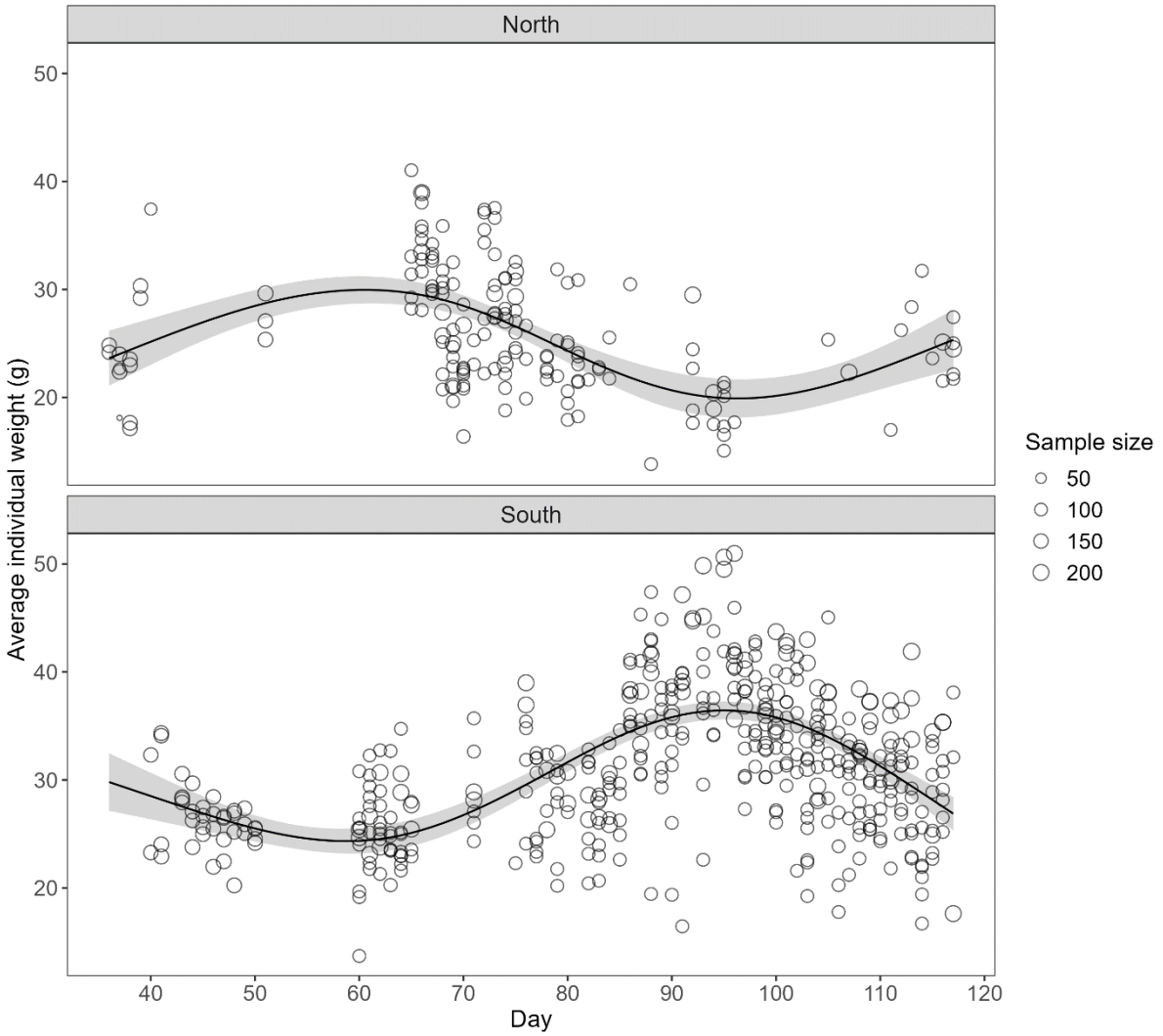

Figure 6. Average individual *D. gahi* weights per haul from FIFD and MRAG observer data (circles) and the fitted GAM trend (black line) with 95% CI (grey shading).

3.3. Depletion model – north sub-area

Model fit

For the north sub-area, the model provided a good fit to the observed catches; note that catches were sparse in the second half of the season (Figure A.1). Parameter estimates (catchability *q*, and number of squid present on the first day of the season *N1*) and MCMC samples from the posterior distribution are given in Appendix (Chapter 5.4, Figure A.2).

MCMC trace plots showed no evident lack of convergence in estimated parameters (Figure A.4). All the MCMC diagnostic tests were passed by the estimated parameters, indicating[b] convergence (Table A.1, Table A.2). No autocorrelation in MCMC samples was observed (Figure A.5).

Biomass estimates

In the north sub-area, the modelled estimated biomass for the first day of the season (March 1st) was 33,225 t (95% CI: 27,158 – 45,084 t); significantly higher than the pre-season survey biomass estimate of 2,677 t (95% CI: 1,319 – 4,857 t) (Figure 7). Given the delayed start of the season and even further delayed start of fishing in the north, it is likely that a substantial immigration occurred sometime during the two weeks between the survey end and the onset of fishing in the area. For the final day of the season (April 27th), estimated *D. gahi* escapement biomass north was 5,541 t (95% CI: 3,401 – 9,724 t) (Figure 8). The highest estimated biomass of the season occurred on the first day, followed by a continuous decline (Figure 9).

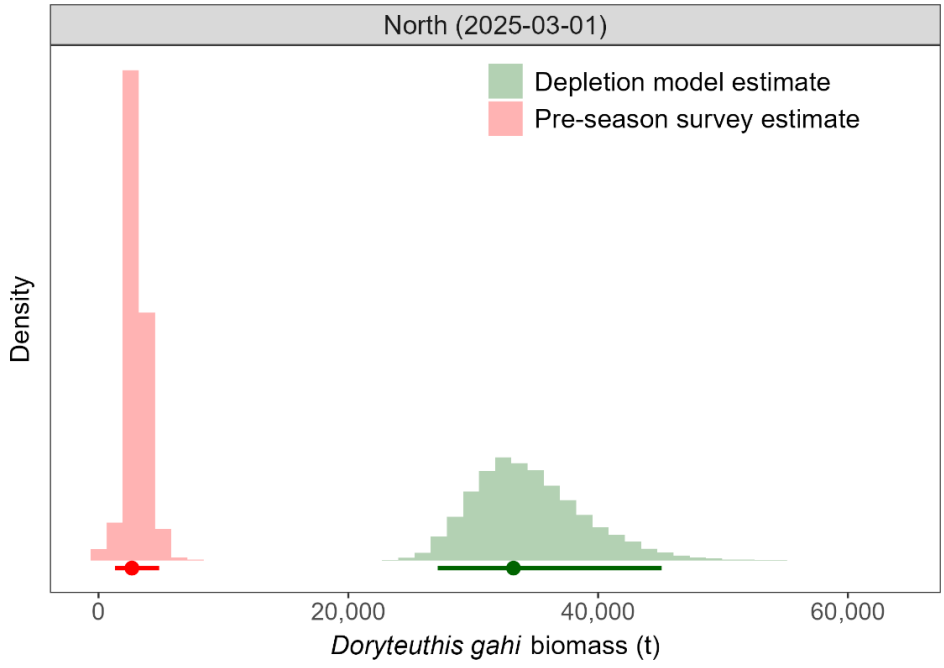

Figure 7. Bootstrapped likelihood distribution of *D. gahi* biomass estimates in the north sub-area from the pre-season survey (red bars) and MCMC posterior distribution from the depletion model for the first day of the season (green bars). Dots: maximum likelihood estimates. Horizontal lines: 95% credible intervals.

[b] It is never possible to say with certainty that a finite sample from an MCMC algorithm is representative of an underlying stationary distribution (Cowles and Carlin 1996).

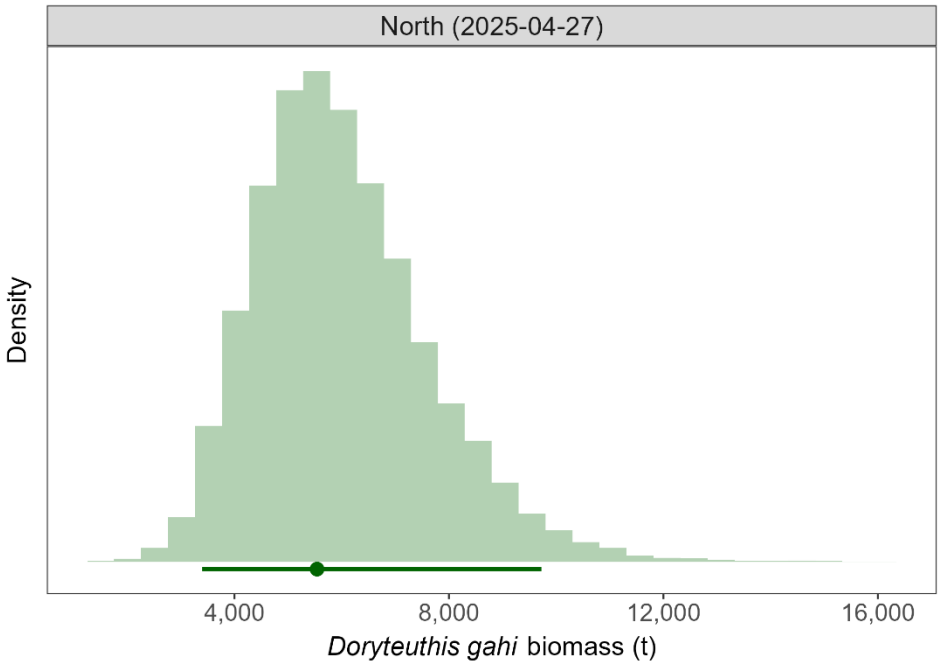

Figure 8. Posterior distribution of *D. gahi* escapement biomass in the north sub-area, at the end of the season. Dot: maximum likelihood estimate. Horizontal line: 95% credible interval.

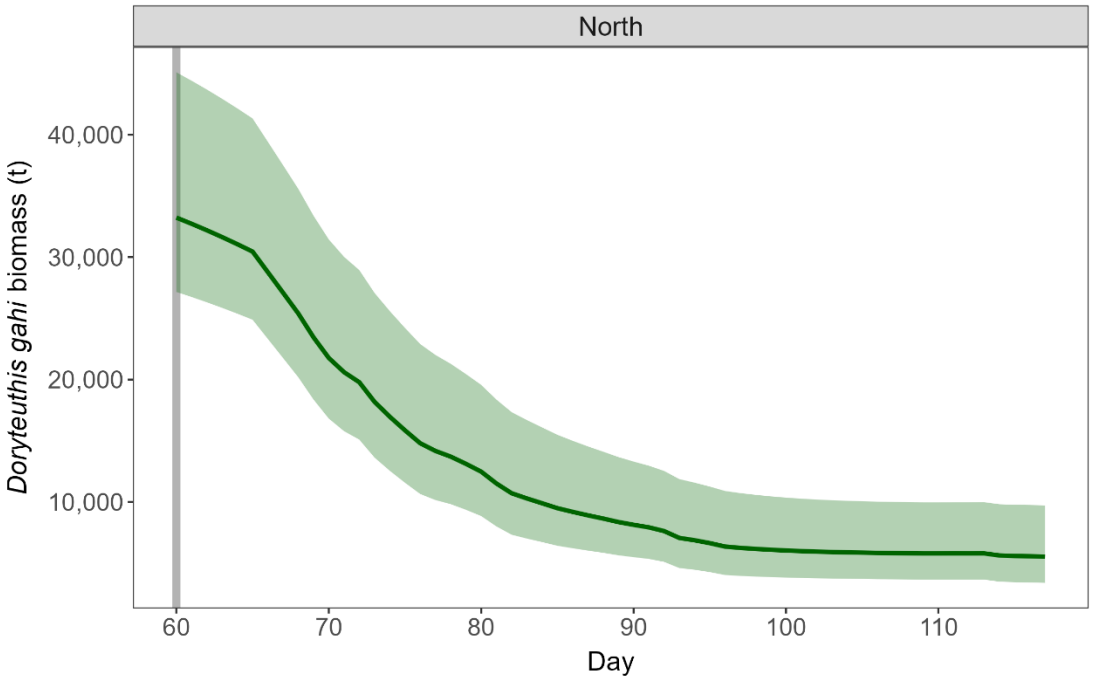

Figure 9. Time series of *D. gahi* biomass estimates in the north sub-area throughout the season. Solid green line: maximum likelihood estimate. Green shading: 95% credible interval. Grey bars: immigration peaks north (day 60).

3.4. Depletion model – south sub-area

Model fit

For the south sub-area, the model provided an adequate fit to the observed catches, especially up to the last immigration peak (Figure A.1). Parameter estimates (catchability *q*, numbers of squid present on the first day of the season *N1* and immigrating on the three subsequent immigration events *N2*, *N3* and *N4*) and MCMC samples from the posterior distribution are given in Appendix (Chapter 5.4, Figure A.3).

MCMC trace plots showed no evident lack of convergence in estimated parameters (Figure A.6). All the MCMC diagnostic tests were passed by all the estimated parameters, indicating convergence (Table A.3 Table A.4). A moderate autocorrelation in MCMC samples for parameters *N2* and *N3* was observed, indicating slow mixing in chains, i.e. chains take a large number of steps to explore the entire target distribution effectively (Figure A.7).

Biomass estimates

In the south sub-area, the modelled estimated biomass for the first day of the season (March 1st) was 23,237 t (95% CI: 16,598 – 33,082 t), not significantly different than the pre-season survey biomass estimate of 28,357 t (95% CI: 24,688 – 39,065 t) (Figure 10). For the final day of the season (April 27th), estimated *D. gahi* escapement biomass south was 10,731 t (95% CI: 7,338 – 16,980 t) (Figure 11). The highest estimated biomass of the season occurred with the fourth immigration peak on day 95, reaching 36,071 t (Figure 12).

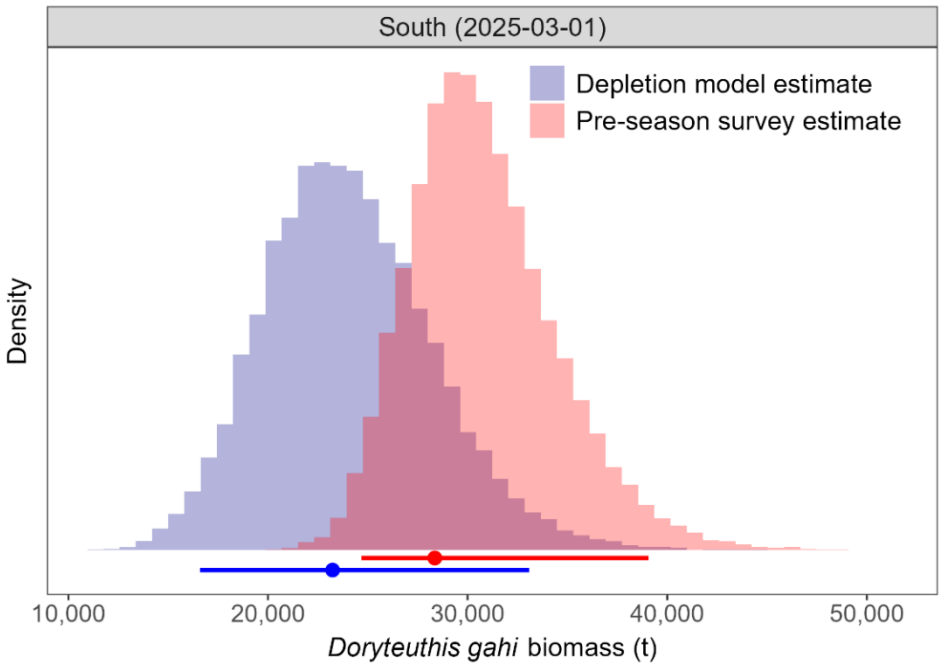

Figure 10. Bootstrapped likelihood distribution of *D. gahi* biomass estimates in the south sub-area from the pre-season survey (red bars) and MCMC posterior distribution from the depletion model for the first day of the season (blue bars). Dots: maximum likelihood estimates. Horizontal lines: 95% CI.

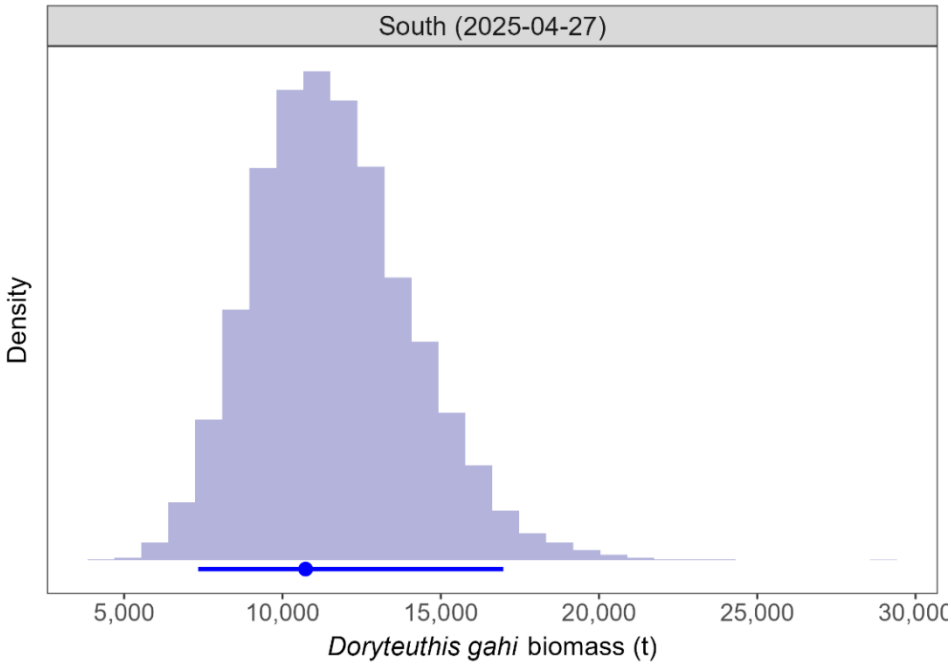

Figure 11. Posterior distribution of *D. gahi* escapement biomass in the south sub-area, at the end of the season. Dot: maximum likelihood estimate. Horizontal line: 95% credible interval.

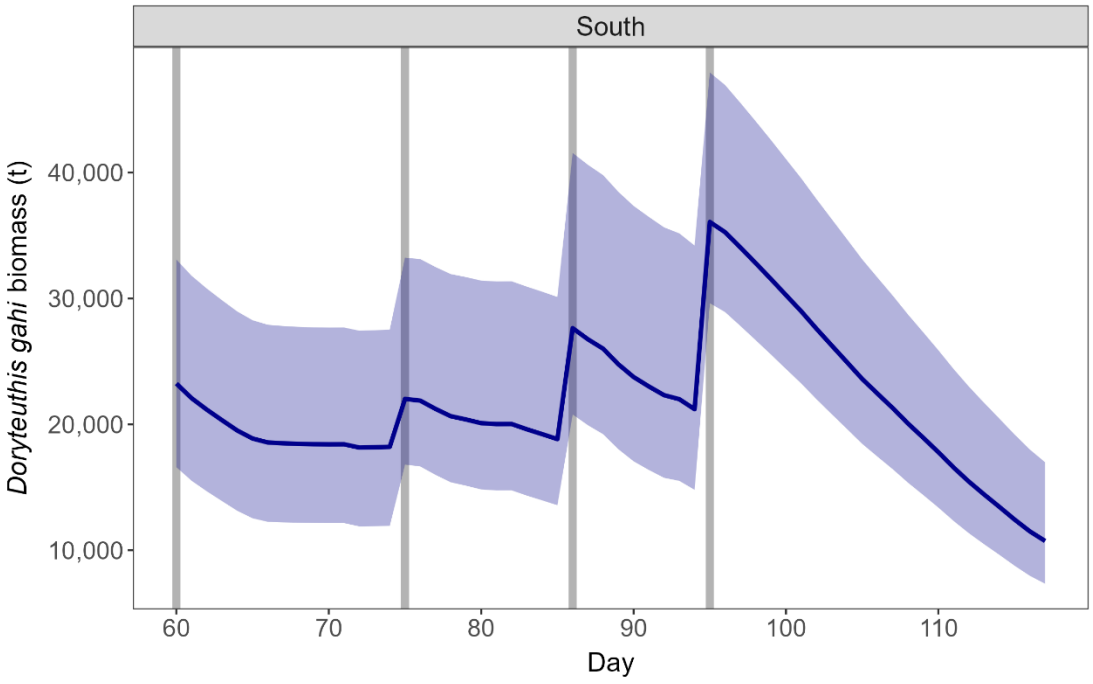

Figure 12. Time series of *D. gahi* biomass estimates in the south sub-area throughout the season. Solid blue line: maximum likelihood estimate. Blue shading: 95% credible interval. Grey bars: immigration peaks south (days 60, 75, 86 and 95).

3.4. Immigration

Doryteuthis gahi immigration during the season was inferred on each day by how many more squid were estimated present than the day before, minus the number caught and the number expected to have died naturally:

$$\mathrm{N_{immigration\ day\ i}} = \mathrm{N_{day\ i}} - \left(\mathrm{N_{day\ i-1}} - \mathrm{C_{day\ i-1}} - \mathrm{M_{day\ i-1}}\right)$$

where $N_{day\ i-1}$ are optimised in the depletion models, $C_{day\ i-1}$ calculated as in Equations **2** and **3**, and $M_{day\ i-1}$ is:

$$\mathrm{M_{day\ i-1}} = \left(\mathrm{N_{day\ i-1}} - \mathrm{C_{day\ i-1}}\right) \times \left(1 - \mathrm{e}^{-\mathrm{M}}\right)$$

Immigration biomass per day was then calculated as the immigration number per day multiplied by the predicted average individual weight. All numbers *N* are themselves derived from the daily average individual weights, therefore the estimation automatically factors in that those squid immigrating on a given day would likely be smaller than average (because younger). Credible intervals of the immigration estimates were calculated by applying the above algorithms to the MCMC iterations of the depletion models.

The resulting total *D. gahi* immigration up to season end was -2,892 t (95% CI: -4,883 – 764 t) in the north and 29,609 t (95% CI: 23,151 – 40,526 t) in the south sub-area. Total (north + south) immigration, with credible interval calculated from the randomised addition of the north and south estimate distributions, was 26,717 t (95% CI: 20,192 – 38,517 t).

In the north sub-area, there were no in-season immigration peaks (start day 60 was de facto not an in-season immigration). A negative immigration value for the season suggests a net emigration from the north sub-area. With no notable in-season immigration peaks, net emigration was a result of minor fluctuations in immigration/emigration throughout the season.

In the south sub-area, the in-season peaks on days 75, 86 and 95 accounted for 12.7%, 31.7% and 52.7% of in-season immigration (start day 60 was de facto not an in-season immigration). The remaining immigration of 2.9% was accounted for by minor fluctuations throughout the season.

3.5. Escapement biomass

Total escapement biomass was defined as the aggregate biomass of *D. gahi* at the end of day 117 (April 27th) for north and south sub-areas combined. Total *D. gahi* escapement biomass, with credible interval calculated from the randomised addition of the north and south posterior distributions, was 16,272 t (95% CI: 12,395 – 24,009 t) (Figure 13).

With both the north and the south escapement biomass distributions being slightly right-skewed (Figures 8 and 11), the addition of the two produced an asymmetric credible interval relative to the maximum likelihood estimate. The risk of the fishery in the current season, defined as the proportion of the total escapement biomass distribution below the conservation limit of 10,000 tonnes (Agnew et al. 2002, Barton 2002), was calculated as <0.1%.

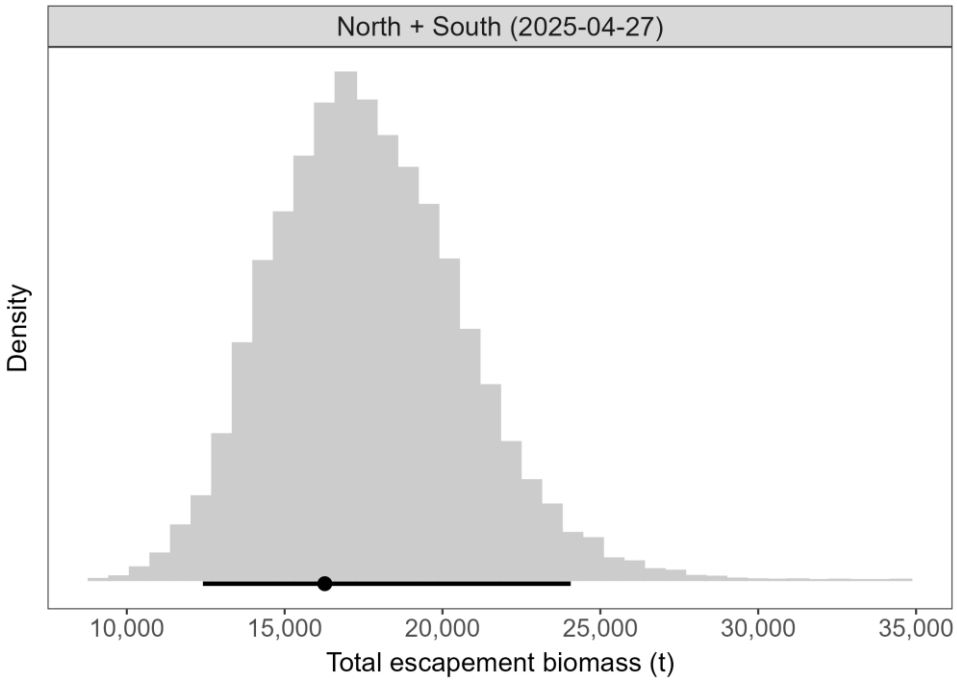

Figure 13. Combined posterior distribution of *D. gahi* escapement biomass north and south at the season end (April 27th). Dot: maximum likelihood estimate. Horizontal line: 95% credible interval.

3.6. Fishery bycatch

All 899 first season vessel-days reported *D. gahi* squid as their primary catch. *D. gahi* represented 95.7% of season total catch. The highest aggregate bycatches in first season 2025 were common rock cod PAR *Patagonotothen ramsayi* with 1,070 tonnes from 885 vessel-days (catch reports), common hake HAK *Merluccius hubbsi* (407 t, 739 v-days), red cod BAC *Salilota australis* (57 t, 280 v-days), frogmouth CGO *Cottoperca gobio* (19 t, 739 v-days), black southern rock cod PTE *Patagonotothen tessellata* (16 t, 312 v-days), Illex squid ILL *Illex argentinus* (14 t, 450 v-days), toothfish TOO *Dissostichus eleginoides* (12 t, 615 v-days), and jellyfish MED Scyphozoa (10 t, 199 v-days). Bycatch distributions by grid square are shown in Figure 14; the complete catch composition is in Table A.5.

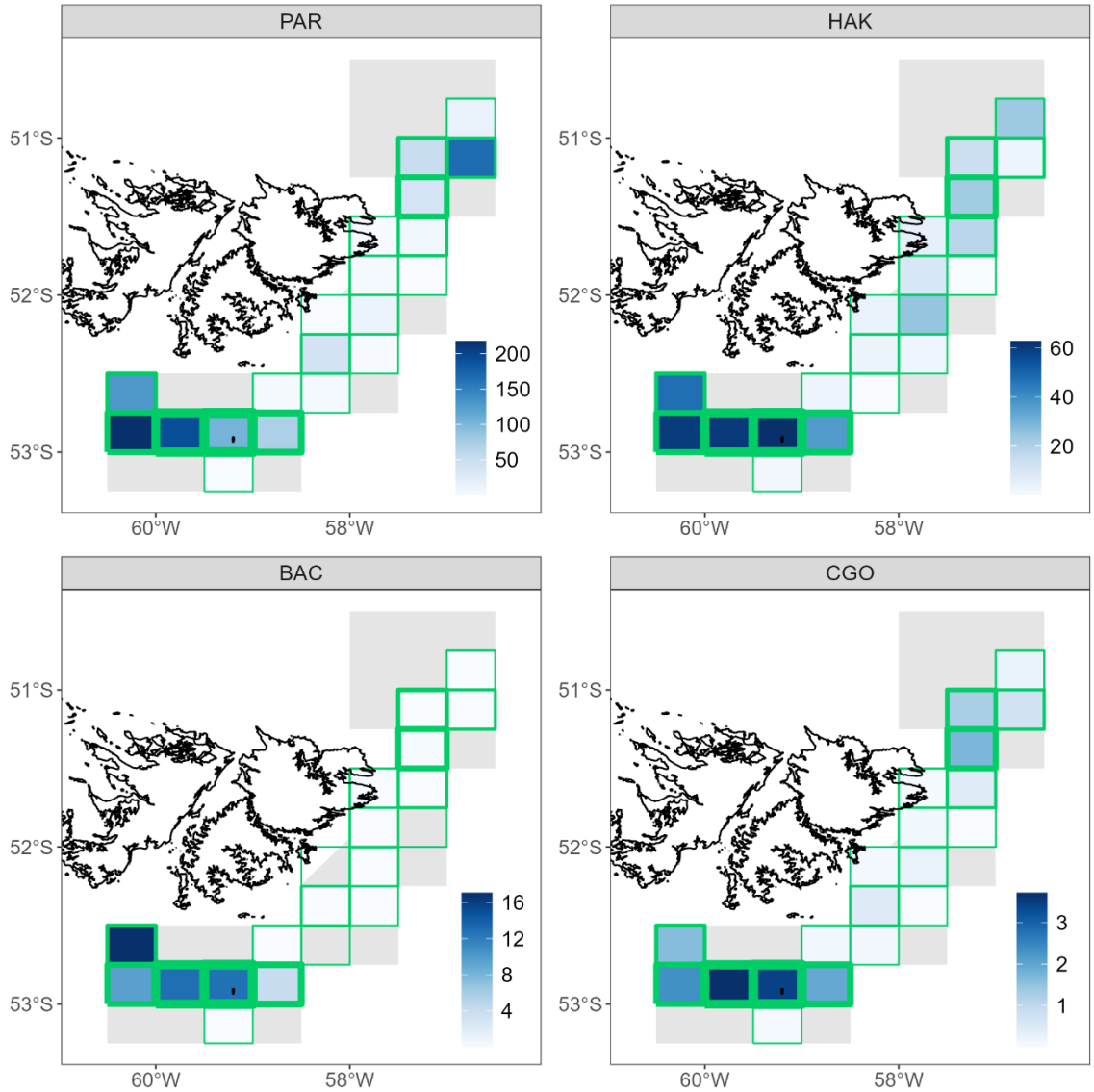

Figure 14. Distributions of the eight main bycatch species catches by grid square in 1st season 2025. Thickness of grid lines is proportional to the number of vessel-days (2 to 172 per grid; 20 different grids were occupied). Blue-scale is proportional to bycatch weight.

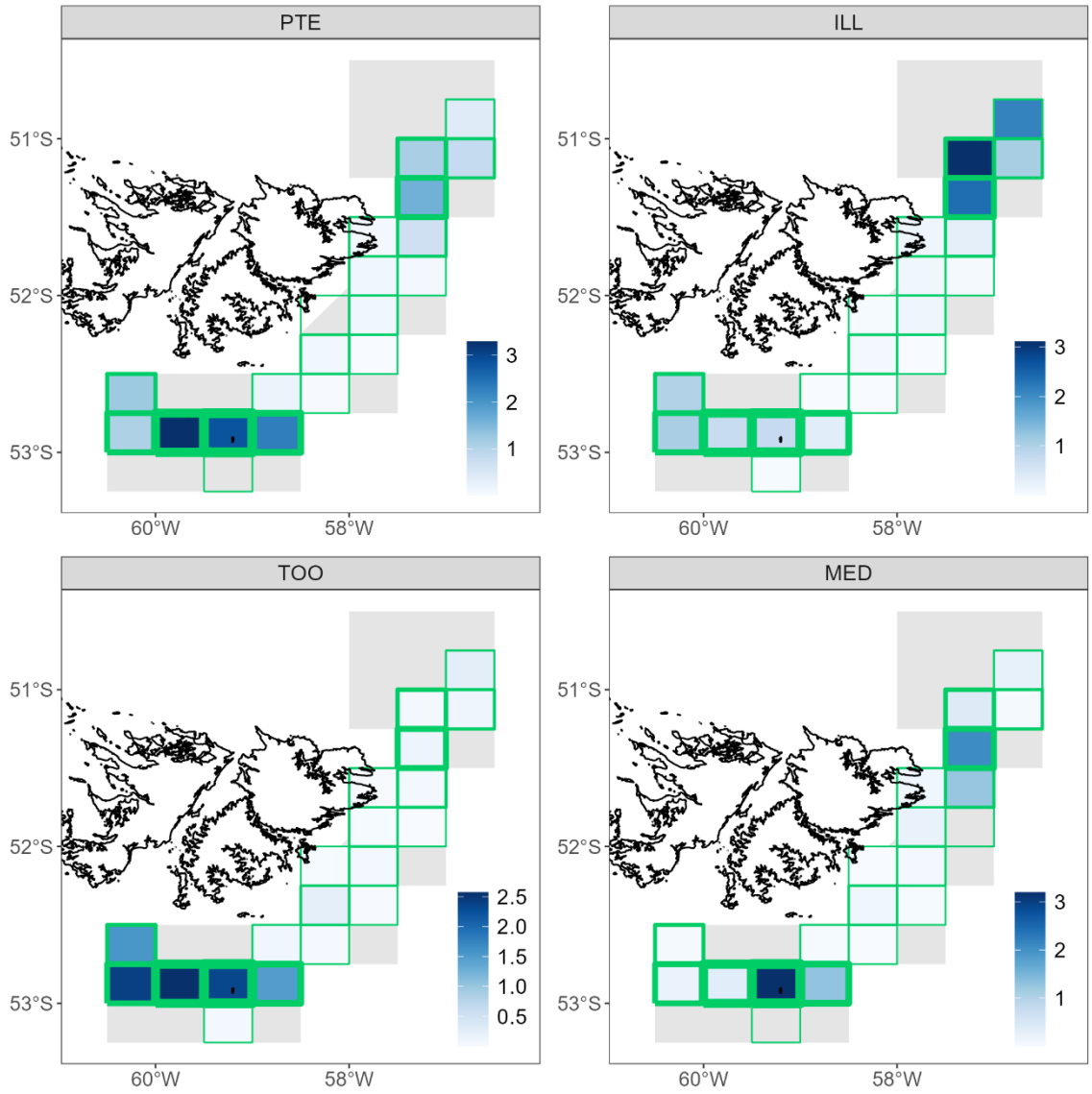

Figure 14. Continued.

4. References

Agnew DJ, Baranowski R, Beddington JR, des Clers S, Nolan CP. 1998. Approaches to assessing stocks of *Loligo gahi* around the Falkland Islands. Fisheries Research 35: 155-169.

Agnew DJ, Beddington JR, Hill S. 2002. The potential use of environmental information to manage squid stocks. Canadian Journal of Fisheries and Aquatic Sciences 59: 1851-1857.

Akaike H. 1973. Information theory and an extension of the maximum likelihood principle. 2nd International Symposium on Information Theory: 267-281.

Amukwaya A. 2025. Observer Report 1427. Technical Document, FIG Fisheries Department. 27p.

Arkhipkin A. 1993. Statolith microstructure and maximum age of *Loligo gahi* (Myopsida: Loliginidae) on the Patagonian Shelf. Journal of the Marine Biological Association of the UK 73: 979-982.

Arkhipkin AI, Middleton DAJ. 2002. Sexual segregation in ontogenetic migrations by the squid *Loligo gahi* around the Falkland Islands. Bulletin of Marine Science 71: 109-127.

Arkhipkin AI, Middleton DAJ, Barton J. 2008. Management and conservation of a short-lived fishery resource: *Loligo gahi* around the Falkland Islands. American Fisheries Society Symposium 49: 1243-1252.

Arkhipkin AI, Hendrickson LC, Payá I, Pierce GJ, Roa-Ureta RH, Robin J-P, Winter A. 2021. Stock assessment and management of cephalopods: advances and challenges for short-lived fishery resources. ICES Journal of Marine Science 78: 714-730.

Barton J. 2002. Fisheries and fisheries management in Falkland Islands Conservation Zones. Aquatic Conservation: Marine and Freshwater Ecosystems 12: 127-135.

Brooks SP, Gelman A. 1998. General methods for monitoring convergence of iterative simulations. Journal of Computational and Graphical Statistics 7: 434-455.

Cowles MK, Carlin BP. 1996. Markov Chain Monte Carlo convergence diagnostics: A comparative review. Journal of the American Statistical Association 91: 883-904.

DeLury DB. 1947. On the estimation of biological populations. Biometrics 3: 145-167.

FIFD. 2004. Fishery Report, *Loligo gahi*, Second Season 2004. Fishing statistics, biological trends, and stock assessment. Technical Document, Falkland Islands Fisheries Department. 15 p.

Gamerman D, Lopes HF. 2006. Markov Chain Monte Carlo. Stochastic simulation for Bayesian inference. 2nd edition. Chapman & Hall/CRC.

Geweke J. 1992. Evaluating the accuracy of sampling-based approaches to calculating posterior moments. In: Bernardo JM, Berger JO, David AP, Smith AFM (Eds.). Bayesian Statistics, 4. Clarendon Press, Oxford, 169-194.

Hamel OS, Cope JM. 2022. Development and considerations for application of a longevity-based prior for the natural mortality rate. Fisheries Research 256: 106477.

Heidelberger P, Welch P. 1983. Simulation run length control in the presence of an initial transient. Operations Research 31: 1109-1144.

Magnusson A, Punt A, Hilborn R. 2013. Measuring uncertainty in fisheries stock assessment: the delta method, bootstrap, and MCMC. Fish and Fisheries 14: 325-342.

Maunder MN, Hamel OS, Lee H-H, Piner KR, Cope JM, Punt AE, Ianelli JN, Castillo-Jordan C, Kapur MS, Methot RD. 2023. A review of estimation methods for natural mortality and their performance in the context of fishery stock assessment. Fisheries Research 257: 106489.

Ongoro F. 2025. Observer Report 1434. Technical Document, FIG Fisheries Department. 30p.
Orlandi N. 2025a. Observer Report 1431. Technical Document, FIG Fisheries Department. 32p.
Orlandi N. 2025b. Observer Report 1435. Technical Document, FIG Fisheries Department. 34p.
Patterson KR. 1988. Life history of Patagonian squid *Loligo gahi* and growth parameter estimates using least-squares fits to linear and von Bertalanffy models. Marine Ecology Progress Series 47: 65-74.
Payá I. 2010. Fishery Report. *Loligo gahi*, Second Season 2009. Fishery statistics, biological trends, stock assessment and risk analysis. Technical Document, Falkland Islands Fisheries Dept. 54 p.
Pierce GJ, Guerra A. 1994. Stock assessment methods used for cephalopod fisheries. Fisheries Research 21: 255-285.
R Core Team. 2022. R: A language and environment for statistical computing. R Foundation for Statistical Computing, Vienna, Austria. http://www.R-project.org/
Roa-Ureta R. 2012. Modelling in-season pulses of recruitment and hyperstability-hyperdepletion in the *Loligo gahi* fishery around the Falkland Islands with generalized depletion models. ICES Journal of Marine Science 69: 1403-1415.
Roa-Ureta R, Arkhipkin AI. 2007. Short-term stock assessment of *Loligo gahi* at the Falkland Islands: sequential use of stochastic biomass projection and stock depletion models. ICES Journal of Marine Science 64: 3-17.
Rosenberg AA, Kirkwood GP, Crombie JA, Beddington JR. 1990. The assessment of stocks of annual squid species. Fisheries Research 8: 335-350.
Shaw PW, Arkhipkin AI, Adcock GJ, Burnett WJ, Carvalho GR, Scherbich JN, Villegas PA. 2004. DNA markers indicate that distinct spawning cohorts and aggregations of Patagonian squid, *Loligo gahi*, do not represent genetically discrete subpopulations. Marine Biology 144: 961-970.
Skeljo F, Winter A. 2024. Stock assessment – Falkland calamari *Doryteuthis gahi* 1st season 2024. Technical Document, Falkland Islands Fisheries Department. 35 p.
Winter A, Arkhipkin A. 2015. Environmental impacts on recruitment migrations of Patagonian longfin squid (*Doryteuthis gahi*) in the Falkland Islands with reference to stock assessment. Fisheries Research 172: 85-95.

5. Appendix

5.1. Catchability prior

The catchability coefficient *q* for the season was defined as the ratio of *L. gahi* CPUE (in numbers per vessel-day) and abundance on the first fishing day of the season (day 60):

$$\mathrm{q} = \frac{\mathrm{CPUE\ (N)}_{60}}{\mathrm{N}_{60}} \quad \textbf{(A1)}$$

The CPUE in numbers per vessel-day was obtained by dividing the CPUE in biomass per vessel-day (reported by the fishery) with the GAM-predicted individual weight average on the first day of the season:

$$\mathrm{CPUE\ (N)}_{60} = \frac{\mathrm{CPUE\ (B)}_{60}}{\bar{\mathrm{w}}_{60}} \quad \textbf{(A2)}$$

The abundance on the first day of the season was calculated as the abundance on the last day of the pre-season survey (day 51) discounted for natural mortality acting over the intervening 9-day period (no fishing occurred during this time):

$$\mathrm{N}_{60} = \mathrm{N}_{51} \times \mathrm{e}^{-\mathrm{M}(60-51)} \quad \textbf{(A3)}$$

The abundance on the last day of the pre-season survey was calculated as the survey biomass divided by the GAM-predicted individual weight average for the survey:

$$\mathrm{N}_{51} = \frac{\mathrm{B\ survey}}{\bar{\mathrm{w}}\ \mathrm{survey}} \quad \textbf{(A4)}$$

Substituting equations **A2, A3** and **A4** into equation **A1** leads to:

$$\mathrm{q} = \frac{\frac{\mathrm{CPUE\ (B)}_{60}}{\bar{\mathrm{w}}_{60}}}{\frac{\mathrm{B\ survey}}{\bar{\mathrm{w}}\ \mathrm{survey}} \times \mathrm{e}^{-9\mathrm{M}}} \quad \textbf{(A5)}$$

Variables w_{60}, w_{survey}, B_{survey} and M were assumed normally distributed, parameterised with the mean and standard deviation obtained from the pre-season survey biomass report (B_{survey}), calculated from the individual *D. gahi* weight data during the pre-season survey (w_{60}, w_{survey}), or adapted from the literature (M):

$$\mathrm{B_{survey}} \sim \mathrm{N}(31{,}034, 10{,}272^{c})$$

[c] Hierarchical bootstrapping of the inverse distance weighting algorithm obtained a coefficient of variation (CV) equal to 11.1% of the survey biomass distribution. From modelled survey catchability, Payá (2010) had estimated average net escapement of up to 22%, which was added to the CV (CV = 11.1% + 22.0% = 33.1%). Standard deviation was then calculated as 31,034 t * 33.1% = 10,272 t. The 22% escapement was added as a linear increase in the variability, but was not used to reduce the total estimate, because squid that escape one trawl are likely to be part of the biomass concentration that is available to the next trawl.

$$\overline{w}_{60} \sim N(0.02508, 0.00050)$$

$$\overline{w}_{survey} \sim N(0.02569, 0.00065)$$

$$M \sim N(0.01534, 0.00487)$$

The prior distribution of *q* was obtained by randomly sampling 100,000 values from the distributions of w_{60}, w_{survey}, B_{survey}, and *M*, and randomly resampling the observed 16 values of $CPUE(B)_{60}$ 100,000 times with replacement, and recalculating *q* from equation **A5**. The resulting distribution of 100,000 *q* values was fitted with gamma and lognormal distributions (appropriate for strictly positive continuous data). The lognormal distribution provided a better fit; therefore, *q* prior was defined as a lognormal distribution parameterised by the mean and standard deviation in log-space:

$$q \sim LOGN(-6.872, 0.476)$$

5.2. Model weighting

Relative weights in the joint optimisation were assigned to Equations **3** and **4** as the converse of their coefficients of variation (CV), i.e., the CV of the prior became the weight of the depletion model and the CV of the depletion model became the weight of the prior.

The CV of the depletion model was calculated as the normalised root mean squared deviation (NRMSD) of the differences between the observed and predicted daily catches in numbers:

$$CV_{model} = NRMSD = \frac{\sqrt{\frac{1}{n}\sum_{i=1}^{n}\left(C_{observed\,i} - C_{predicted\,i}\right)^2}}{\overline{C_{observed\,i}}}$$

The CV of the lognormal prior was calculated as:

$$CV_{prior} = \sqrt{e^{\sigma^2} - 1}$$

where σ is the standard deviation in log-space. The CV_{model} was calculated separately for the south and north sub-area depletion models. As the prior of *q* was defined for the north and south sub-areas combined, the CV_{prior} was shared by the two sub-areas models.

5.3. Model fit

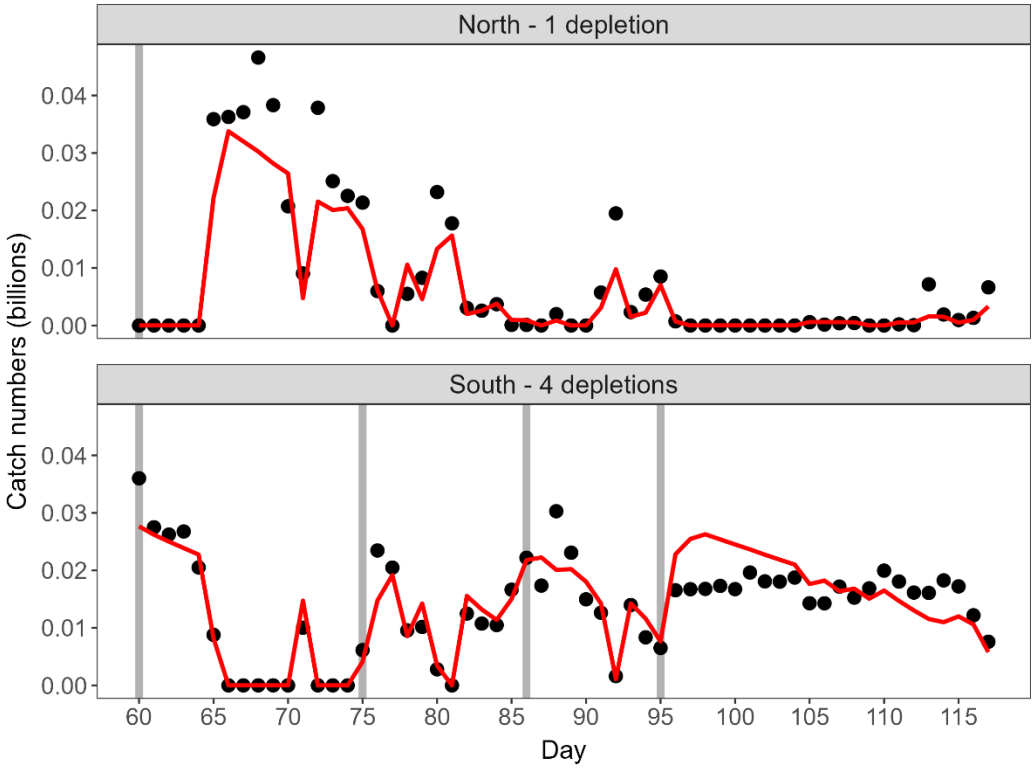

Figure A.1. Daily catch numbers estimated from actual catch (black dots) and predicted from the depletion model in the north and south sub-area (red lines). Solid grey bars indicate the starts of in-season depletions north (day 60) and south (days 60, 75, 86 and 95).

5.4. Parameter estimates

For the north sub-area, joint optimisation of Equations **3** and **4** resulted in parameters values: $N1_{(\text{day } 60)} = 1.109 \times 10^9$, and $q = 2.179 \times 10^{-3}$. Posterior distributions of estimated parameters for the north sub-area are given in Figure A.2. Posterior distribution of q was much narrower than its prior distribution, suggesting that the data were informative about q.

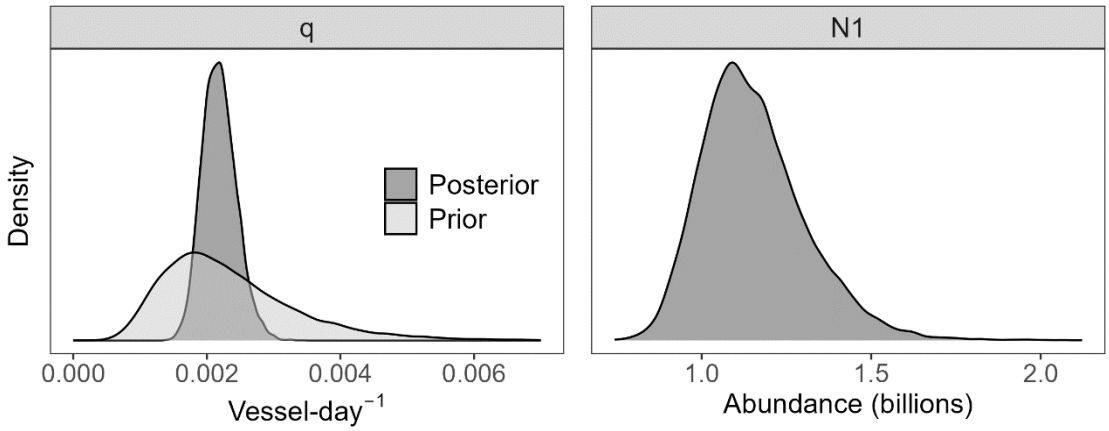

Figure A.2. Prior (light grey) and posterior distributions (dark grey) of estimated parameters for the north sub-area. Note that only catchability q has a prior (the same for north and south).

For the south sub-area, joint optimisation of Equations **3** and **4** resulted in parameter estimates: $N1_{(\text{day } 60)} = 0.954 \times 10^9$, $N2_{(\text{day } 75)} = 0.130 \times 10^9$, $N3_{(\text{day } 86)} = 0.274 \times 10^9$, $N4_{(\text{day } 95)} = 0.425 \times 10^9$, and $q = 1.826 \times 10^{-3}$. Posterior distributions of estimated parameters are given in Figure A.3. Posterior distribution of q was much narrower than its prior distribution, suggesting that the data were informative about q.

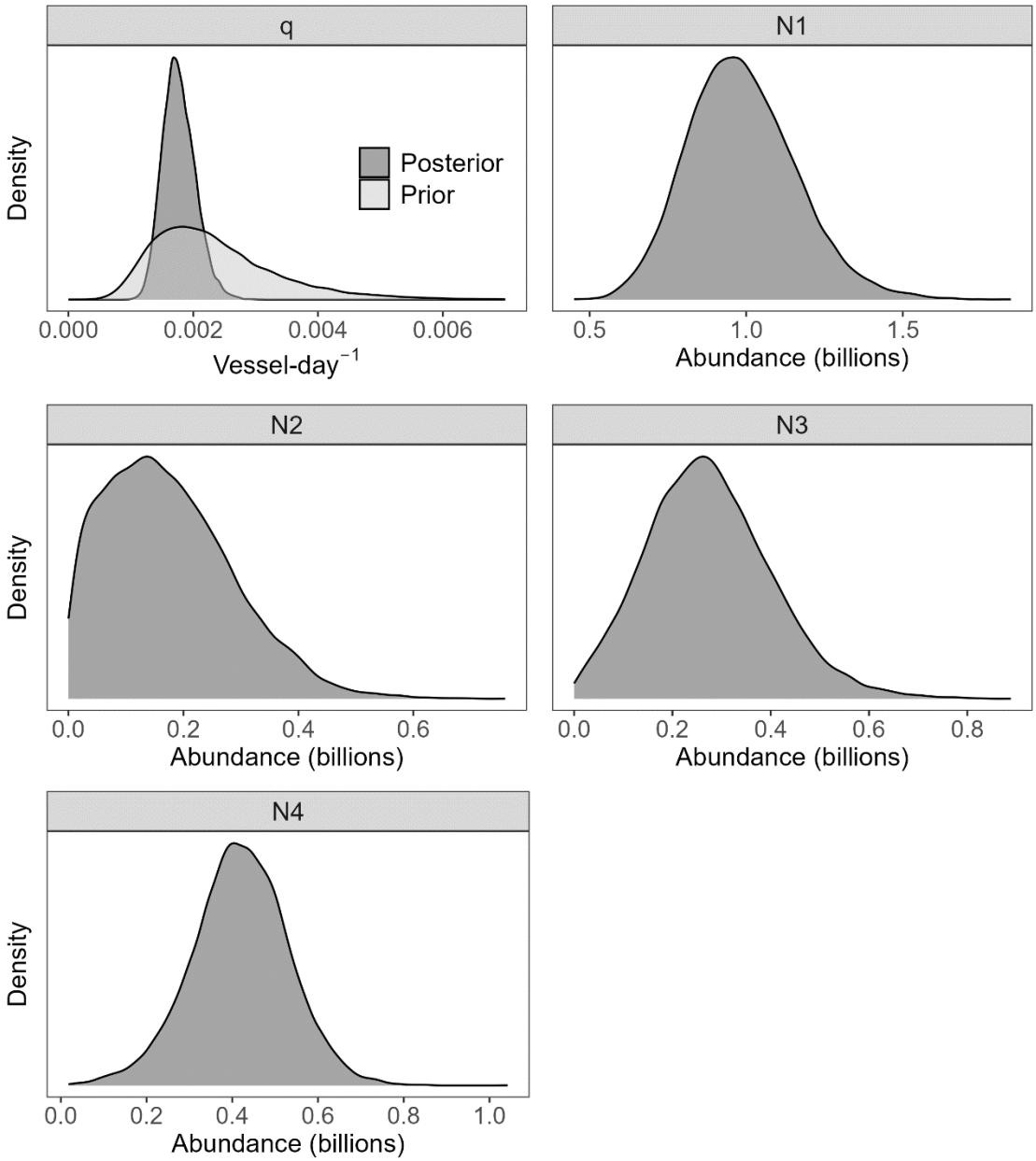

Figure A.3. Prior (light grey) and posterior distributions (dark grey) of estimated parameters for the south sub-area. Note that only catchability *q* has a prior (the same for south and north).

5.5. Model diagnostics

North sub-area

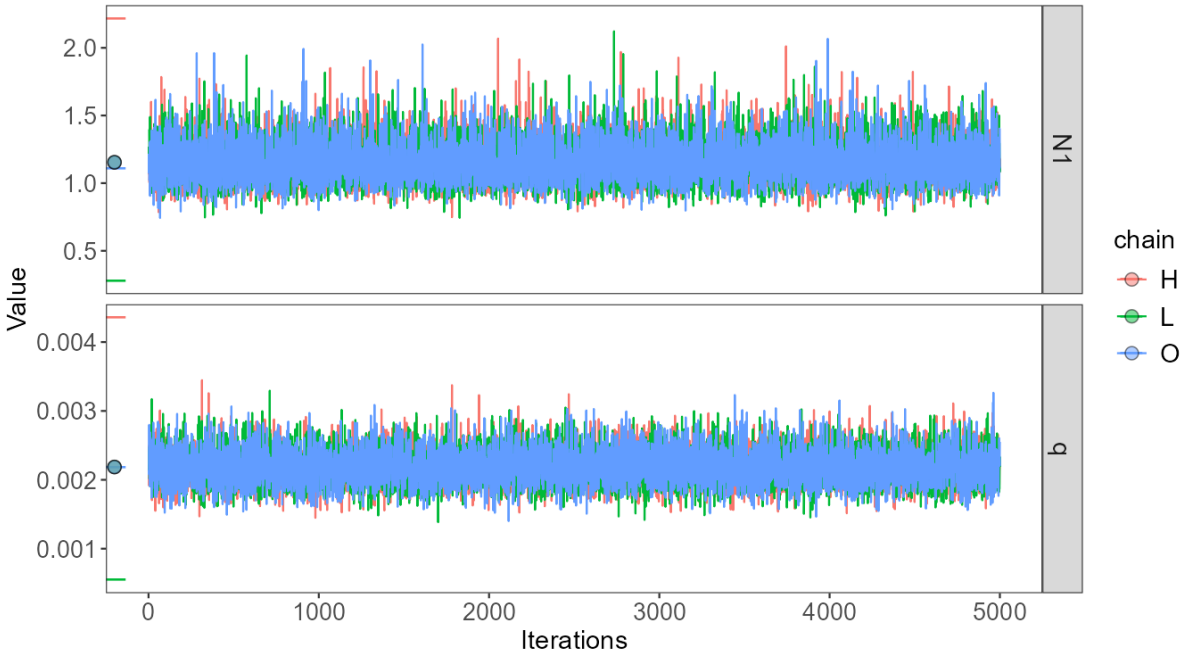

Figure A.4. MCMC posterior trace plots for the estimated parameters, after burn-in and thinning. Colours denote chains initiated at different starting values (H – high, L – low, O – optimal). Horizontal line segments: starting values of the three chains. Dots: mean values of the three chains.

Table A.1. MCMC convergence diagnostic results: Geweke's single-chain stationarity test and Heidelberger and Welch's stationarity and half-width tests.

Parameter	Chain	Geweke's stationarity test		Heidelberger and Welch's stationarity test		Heidelberger and Welch's halfwidth test		
		p-value	outcome	p-value	outcome	mean	halfwidth	outcome
N1	H	0.479	passed	0.883	passed	1.153	0.004	passed
	L	0.674	passed	0.241	passed	1.155	0.004	passed
	O	0.067	passed	0.076	passed	1.154	0.004	passed
q	H	0.546	passed	0.368	passed	0.002	0	passed
	L	0.52	passed	0.701	passed	0.002	0	passed
	O	0.596	passed	0.521	passed	0.002	0	passed

Table A.2. MCMC convergence diagnostic results: Gelman and Rubin's convergence diagnostic for parallel chains.

Parameter	Gelman-Rubin convergence diagnostic ($\hat{R}$)	Convergence ($\hat{R} < 1.1$)	Multivariate version $\hat{R}$	Convergence ($\hat{R} < 1.1$)
N1	1.000098	passed	0.000511	passed
q	1.000086	passed		

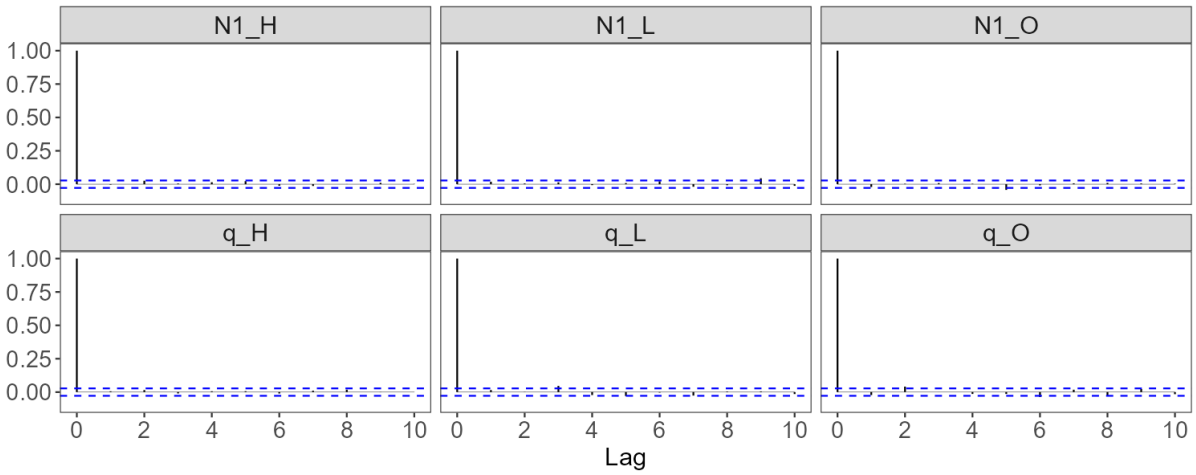

Figure A.5. MCMC autocorrelation lag plots for the estimated parameters.

South sub-area

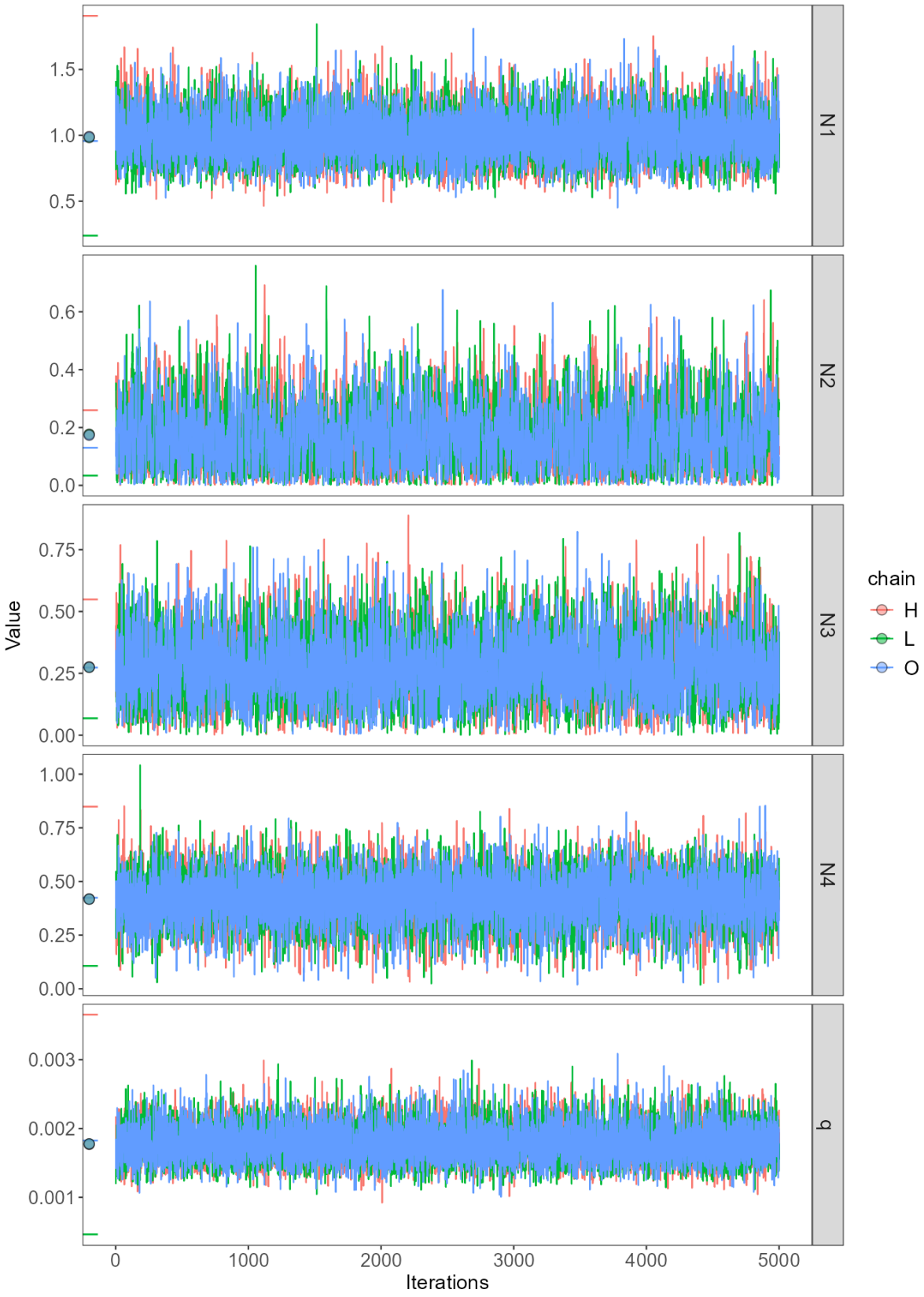

Figure A.6. MCMC posterior trace plots for the estimated parameters, after burn-in and thinning. Colours denote chains initiated at different starting values (H – high, L – low, O – optimal). Horizontal line segments: starting values of the three chains. Dots: mean values of the three chains.

Table A.3. MCMC convergence diagnostic results: Geweke's single-chain stationarity test and Heidelberger and Welch's stationarity and half-width tests.

Parameter	Chain	Geweke's stationarity test		Heidelberger and Welch's stationarity test		Heidelberger and Welch's halfwidth test		
		p-value	outcome	p-value	outcome	mean	halfwidth	outcome
N1	H	0.25	passed	0.493	passed	0.99	0.005	passed
	L	0.178	passed	0.783	passed	0.982	0.006	passed
	O	0.871	passed	0.627	passed	0.988	0.006	passed
N2	H	0.941	passed	0.734	passed	0.176	0.008	passed
	L	0.281	passed	0.649	passed	0.177	0.007	passed
	O	0.42	passed	0.904	passed	0.173	0.007	passed
N3	H	0.295	passed	0.375	passed	0.276	0.005	passed
	L	0.516	passed	0.563	passed	0.274	0.005	passed
	O	0.604	passed	0.191	passed	0.275	0.005	passed
N4	H	0.206	passed	0.288	passed	0.418	0.004	passed
	L	0.685	passed	0.319	passed	0.418	0.004	passed
	O	0.3	passed	0.187	passed	0.418	0.004	passed
q	H	0.201	passed	0.121	passed	0.002	0	passed
	L	0.713	passed	0.969	passed	0.002	0	passed
	O	0.359	passed	0.884	passed	0.002	0	passed

Table A.4. MCMC convergence diagnostic results: Gelman and Rubin's convergence diagnostic for parallel chains.

Parameter	Gelman-Rubin convergence diagnostic ($\hat{R}$)	Convergence ($\hat{R} < 1.1$)	Multivariate version $\hat{R}$	Convergence ($\hat{R} < 1.1$)
N1	1.000464	passed		
N2	1.001030	passed		
N3	1.000011	passed	1.001040	passed
N4	1.000006	passed		
q	1.000115	passed		

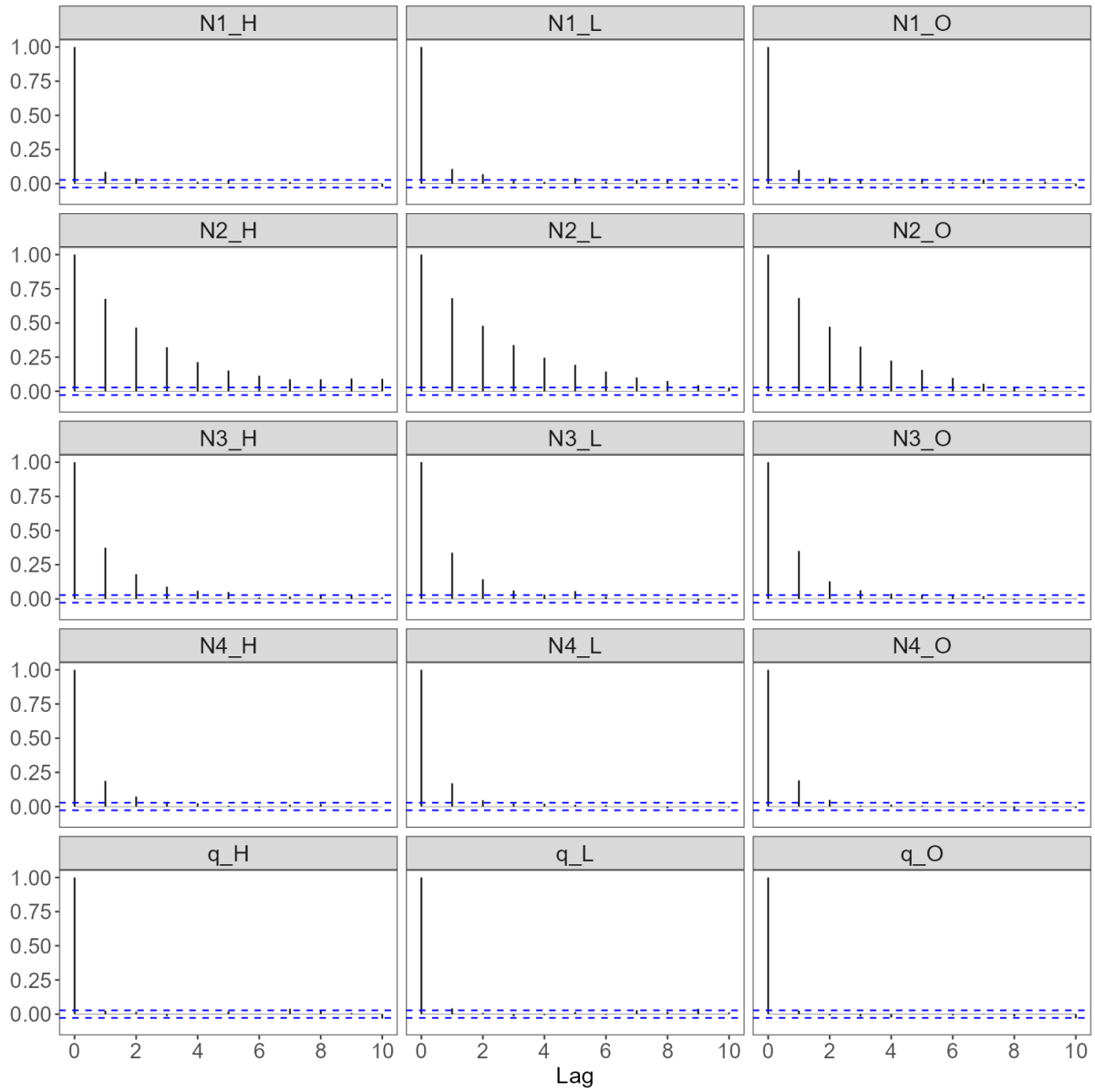

Figure A.7. MCMC autocorrelation lag plots for the estimated parameters.

5.6. Catch composition

Table A.5. Total reported catch and discard by taxon during 1st season 2025 C-license fishing, and percentage of vessel-days in which each taxon occurred. Does not include incidental catches of pinnipeds or seabirds.

Species Code	Species / Taxon	Catch (kg)	Discard (kg)	Occurrence (%)
LOL	*Doryteuthis gahi*	37,492,045	49,530	100.0
PAR	*Patagonotothen ramsayi*	1,070,067	1,067,275	98.4
HAK	*Merluccius hubbsi*	406,866	36,608	82.2
BAC	*Salilota australis*	56,876	6,514	31.1
CGO	*Cottoperca gobio*	18,800	18,760	82.2
PTE	*Patagonotothen tessellata*	16,319	16,319	34.7
ILL	*Illex argentinus*	13,590	6,748	50.1
TOO	*Dissostichus eleginoides*	11,591	11,493	68.4
OTH	Actinopterygii	11,231	11,168	13.9
MED	Scyphozoa	9,782	9,782	22.1
ZYP	*Zygochlamys patagonica*	8,918	8,918	27.3
RAY	Rajiformes	7,579	7,062	56.8
KIN	*Genypterus blacodes*	7,282	1,970	18.1
BLU	*Micromesistius australis*	5,210	2,561	7.0
ING	*Moroteuthopsis ingens*	3,853	3,853	38.7
DGH	*Schroederichthys bivius*	3,797	3,797	42.5
LIT	*Lithodes turkayi*	3,653	3,568	11.3
LIM	*Lithodes murrayi*	3,599	3,599	11.0
CRB	*Lithodes* sp.	2,169	2,169	6.2
GRV	*Macrourus* spp.	1,858	1,858	11.8
OCT	*Eledone* spp.	1,612	1,612	19.1
UCH	*Strongylocentotus* spp.	1,029	1,029	6.5
EEL	*Iluocoetes fimbriatus*	832	832	12.1
CHE	*Champsocephalus esox*	717	717	10.6
ALF	*Allothunnus fallai*	581	581	6.1
PAT	*Merluccius australis*	304	304	4.0
WHI	*Macruronus magellanicus*	201	201	6.9
SPN	Spongiidae	186	186	1.3
GRF	*Coelorinchus fasciatus*	172	172	1.2
DGS	*Squalus acanthias*	166	166	4.0
COP	*Congiopodus peruvianus*	152	152	2.6
AST	Asteroidea	142	142	2.1
MYX	Myxinidae	83	83	6.5
POR	*Lamna nasus*	80	80	0.1
RED	*Sebastes oculatus*	80	80	3.9
NEM	*Psychrolutes marmoratus*	42	42	1.9
MUL	*Eleginops maclovinus*	41	41	1.2
BUT	*Stromateus brasiliensis*	28	28	0.9
SAR	*Sprattus fuegensis*	25	25	0.6
MUN	*Grimothea gregaria*	22	22	0.7
NOW	*Paranotothenia magellanica*	3	3	0.3
Total		39,161,583	1,280,050	